



PERGAMON

Journal of South American Earth Sciences 16 (2003) 91–106

Journal of
South American
Earth Sciences

www.elsevier.com/locate/james

Composition, provenance, and tectonic setting of Ordovician siliciclastic rocks in the San Rafael block: Southern extension of the Precordillera crustal fragment, Argentina

Carlos Alberto Cingolani*, Marcelo Manassero, Paulina Abre

Centro de Investigaciones Geológicas y Departamento Geología, Universidad Nacional de La Plata-CONICET, calle 1 n. 644, 1900 La Plata, Argentina

Abstract

Sandstone petrography, geochemistry (major, trace, and rare earth elements [REE]), and Nd isotopic composition are presented for the siliciclastic Lower Caradoc Pavón Formation of the San Rafael block, central west Argentina. These constrain the provenance and tectonic setting of deposition and enable comparison to equivalent Ordovician units along the proto-Andean Gondwana margin. Most of the Pavón Formation sandstones are quartz-feldspathic wackes, composed of quartz, feldspars, and fragments of metaquartzitic rocks. The samples plot in the recycled orogen and continental block provenance fields of QFL diagrams. In view of the intense recycling and diagenetic processes, as indicated by CIA and CIW indices, diagrams involving immobile trace elements are considered better source indicators and suggest an active margin and island continental arc provenance. REE element distributions and initial ϵ_{Nd} isotopic values (-3.1 to -4.0) provide evidence of upper crust source materials. Nd T_{DM} model ages for the provenance protolith are 1.4 – 1.5 Ga, consistent with a possible sediment source in Grenville-age rocks exposed in the Ponon Trehue area. The Pavón Formation was part of the sedimentary infill of a foreland basin generated and uplifted following accretion of the Precordillera terrane with the Gondwana active margin.

© 2003 Elsevier Science Ltd. All rights reserved.

Keywords: Gondwana margin; Sedimentary geochemistry; Siliciclastic rocks; Upper Ordovician

1. Introduction

The combination of petrography, geochemistry, and Nd isotope data can reveal the nature of source regions and the tectonic setting of sedimentary basins. It also provides insight into the evolution of crustal processes (e.g. Dickinson and Suczek, 1979; Valloni and Mezzardi, 1984; Bhatia and Crook, 1986; McLennan et al., 1993). However, some geochemical ratios can be altered during weathering and/or diagenesis (Nesbitt and Young, 1989; Milodowski and Zalasiewicz, 1991). As long as the bulk composition of a rock is not altered, geochemical analysis is a valuable tool in the study of matrix-rich sandstones (McLennan et al., 1993). Nd isotopic data provide a model age of crustal precursor material and can be used to delineate terrane boundaries or isotopic domains. Exotic sources would strongly indicate the presence of a terrane boundary, whereas homogeneous data may indicate recycling of

preexisting material. Alternatively, juvenile arc material should be recognizable by its radiogenic Nd isotopes, lower Th/Sc ratios, pronounced negative Nb and Ta anomalies, and often less pronounced negative Eu anomalies compared with typical upper crustal compositions (McLennan et al., 1993).

We have studied the siliciclastic sequence of the San Rafael block, Pavón Formation, in the central western Mendoza Province, Argentina (Fig. 1). Its biostratigraphic position (Upper Ordovician) and lithofacies are well known (Cuerda and Cingolani, 1998; Manassero et al., 1999), and preliminary geochemical results have been presented (Cingolani et al., 2002). The San Rafael block is considered a southern extension of the Precordillera terrane and, together with other such belts (e.g. Angaco-Pie de Palo and Las Matras), constitutes the Cuyania composite terrane (Ramos et al., 1998) or the belt with Grenvillian-age rocks (Sato et al., 2000) of western Argentina (Fig. 1). The association of Grenville-age rocks with Lower Paleozoic platform carbonates is the most characteristic feature of the Precordillera terrane.

The main purpose of this work is to evaluate the sandstone petrography, geochemistry (major, trace, and rare

* Corresponding author. Tel.: +54-221-4215677; fax: +54-221-4258696.

E-mail addresses: ccingola@cig.museo.unlp.edu.ar (C.A. Cingolani), paulinabre@yahoo.com.ar (P. Abre).

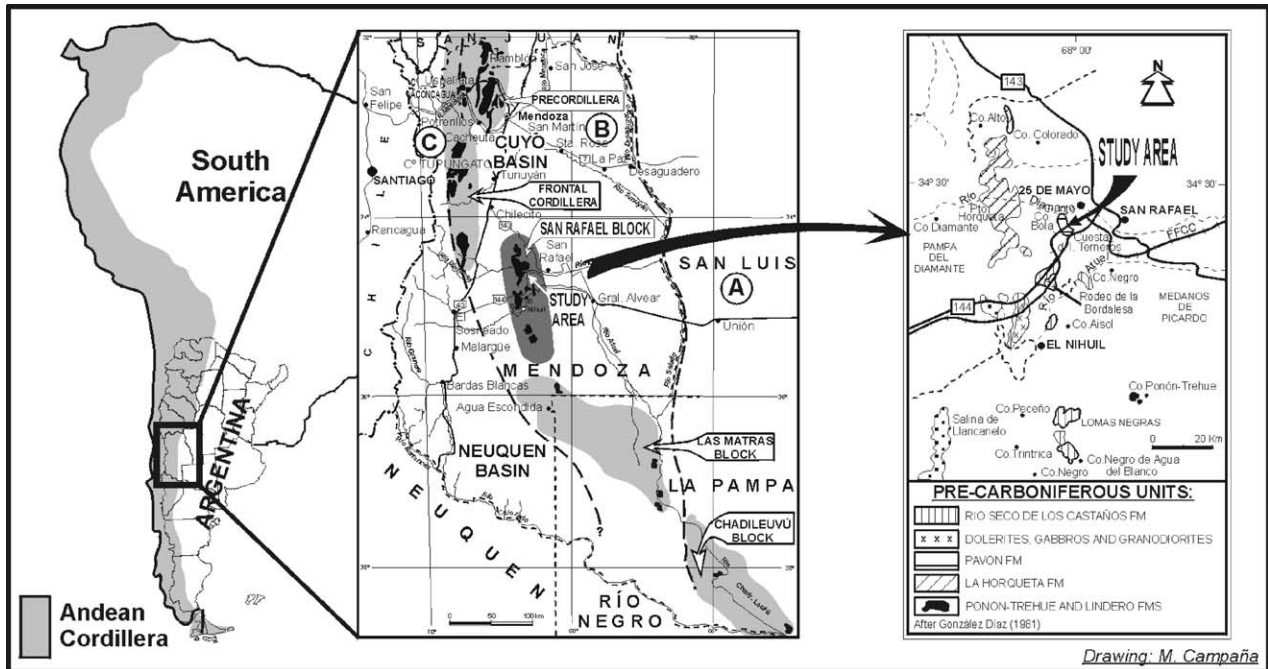


Fig. 1. Location of the study area in the San Rafael block in central western Mendoza Province, western Argentina. The San Rafael block shows a NNW–SSE structural trend and is considered a southward extension of the Precordillera thrust fold belt, from which it is separated by the Cuyo sedimentary basin. The pre-Carboniferous outcrops of different geological units are represented in black: A = Famatinian orogen; B = Precordillera terrane, and C = Chilean terrane. B and C correspond to the Occidentalia terrane (Dalla Salda et al., 1992). The sketch map on the right shows pre-Carboniferous outcrops in the San Rafael block.

earth elements [REE]), and Nd isotopic composition of the Pavón Formation to provide information on the provenance of detrital material and constrain the tectonic setting and continental evolution. These data could be useful to discuss relationships with equivalent Ordovician units located along the proto-Andean Gondwana margin, such as those in the Puna, Famatina, and Precordillera terranes (Merodio and Spalletti, 1990; Loske, 1992; Bahlburg, 1998; Zimmermann and Bahlburg, 1999; Zimmermann, 2000). This contribution is part of a major project to model the source areas and depositional history of Precordilleran Lower Paleozoic units in central western Argentina.

2. Geological setting

Various geotectonic models have been presented to explain the evolution of the Lower Paleozoic of the western Gondwana margin. There is a certain consensus that the Argentine Precordillera, as an exotic or displaced crustal fragment, accreted to the western Gondwana active margin during the Ordovician (Ramos et al., 1986; Dalla Salda et al., 1992; Astini et al., 1995) or Devonian (Keller, 1999) or displaced during the Ordovician–Devonian (Aceñolaza et al., 2002). The Precordillera terrane is characterized by a Grenvillian-type basement overlain by carbonate platform rocks of Cambrian–Ordovician age. According to Astini et al. (1995) and Ramos (1999), during the Late Ordovician, siliciclastic detritus was deposited as a marine clastic wedge

within a foreland basin, after drowning of the Cambrian–Early Ordovician carbonate platform.

The San Rafael block, as the southern extension of the Precordillera terrane (Fig. 1), shows a NNW–SSE structural trend. It is located 200 km south of the Precordillera outcrops in Mendoza Province. Its northern and western sides are bounded by the Cuyo and Neuquén petroliferous basins, respectively. To the east, the San Rafael block loses relief and vanishes beneath Cenozoic sedimentary cover. To the south, it is connected with the Las Matras block (Sato et al., 2000).

The San Rafael block consists of diverse igneous–metamorphic and sedimentary units of Precambrian–Middle Paleozoic age, known generally as pre-Carboniferous units because of their clear differentiation below a Carboniferous regional unconformity (Núñez, 1979; González Díaz, 1981). A Grenvillian-type crust (Cingolani and Varela, 1999; Thomas et al., 2000) is present in the eastern part of the San Rafael block, partially covered by calcareous–siliciclastic sedimentary rocks bearing Ordovician macro- and microfossils (Núñez, 1979; Bordonaro et al., 1996; Heredia, 1996; Astini, 2002). Siliciclastic turbidites of pre-Lower Devonian age are recognized in isolated outcrops (La Horqueta Formation; Dessanti, 1956), as are shallow water sequences bearing ichnofossils of Silurian–Devonian age (Río Seco de los Castaños Formation; González Díaz, 1981; Poiré et al., 2002). Ordovician dolerite dykes (K–Ar age of c. 450 Ma) cut deformed gabbros and tonalites in the Nihuil region, and a small Lower Devonian tonalitic–granodioritic body intrudes

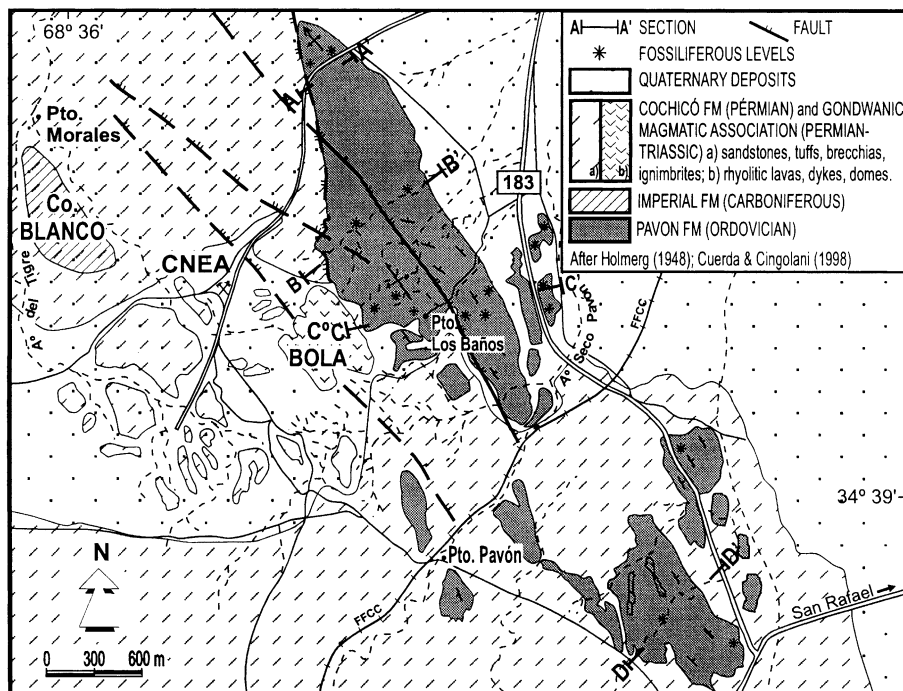


Fig. 2. The Pavón Formation outcrops in the eastern slope of Cerro Bola, and the location of the studied geological sections.

the Horqueta Formation at Rodeo de la Bordalesa (see pre-Carboniferous units in Fig. 1).

In the central portion of the San Rafael block, on the eastern slope of Cerro Bola ($68^{\circ}30'W$, $34^{\circ}35'S$), outcrops of the Pavón Formation cover an area 3.5 km long and 1.2 km (maximum) wide. This unit is composed of folded siliciclastic sediments intruded by Permian–Triassic magmatic rocks and covered by Permian volcaniclastic rocks (Fig. 2).

3. Stratigraphy and age of the Pavón Formation

Holmberg (1948) first studied the region in detail and assigned the Estratos del Arroyo Pavón to the Carboniferous. Dessanti (1945, 1956) mapped these rocks as part of a regional geological survey (Hoja 27c, Cerro Diamante), named them ‘Serie de la Horqueta,’ and suggested that they accumulated between the Precambrian and the Lower Paleozoic. Marquat and Menéndez (1985) identified graptolites in the black shales of the unit. Cuerda and Cingolani (1998), Cuerda et al. (1998) and Cingolani et al. (1999), and Manassero et al. (1999) summarized the stratigraphy of this Ordovician sedimentary succession as follows: It consists of a 700 m thick association of massive green-reddish-grey sandstones, wackes, quartz sandstones, siltstones, and interbedded black shales. The base of the Pavón Formation is not exposed. The X-ray diffraction (XRD) analysis of the shales suggest anchimetamorphic conditions. Tectonic deformation affected some clasts, which produced cleavage, elongation of graptolites, and siliceous recrystallization.

The Pavón Formation is intruded by Permo-Triassic rhyolitic dykes approximately 2–3 m thick and thin hydrothermal quartz veins.

A rich Ordovician graptolite fauna composed of 23 taxa (families Glossograptidae, Nemagraptidae, Dicranograptidae, Diplograptidae, Orthograptidae, Lasiograptidae, and Retiolitidae) has been found in several levels of the Pavón Formation (Cuerda and Cingolani, 1998). The presence of *Climacograptus bicornis* and *C. tridentatus* indicates an Early Caradoc age (*C. bicornis* biozone). On the basis of these assemblages, the Pavón Formation may be correlated with equivalent Precordilleran units (e.g. Empozada, Portezuelo Tontal, Sierra de la Invernada, Las Plantas, La Cantera).

4. Areal distribution of the Pavón Formation facies

Cingolani et al. (1999, 2002) and Manassero et al. (1999) summarize distinctive stratigraphic and sedimentological characteristics of the Pavón Formation, including sand-dominated facies, regular tabular bedding with sharp contacts, scarce flow and load casts at the base of the beds, and rare channels and syn-depositional deformation structures (Fig. 3a and b). A simplified sedimentary model based on non-fan, sandy, marine turbidites (Einsele, 1991) has been suggested by Manassero et al. (1999) to show the relative position of the studied sections along a constructional continental slope. The progradational system of the Pavón Formation produced important vertical (rather than lateral) facies changes, which suggests deposition in a linear

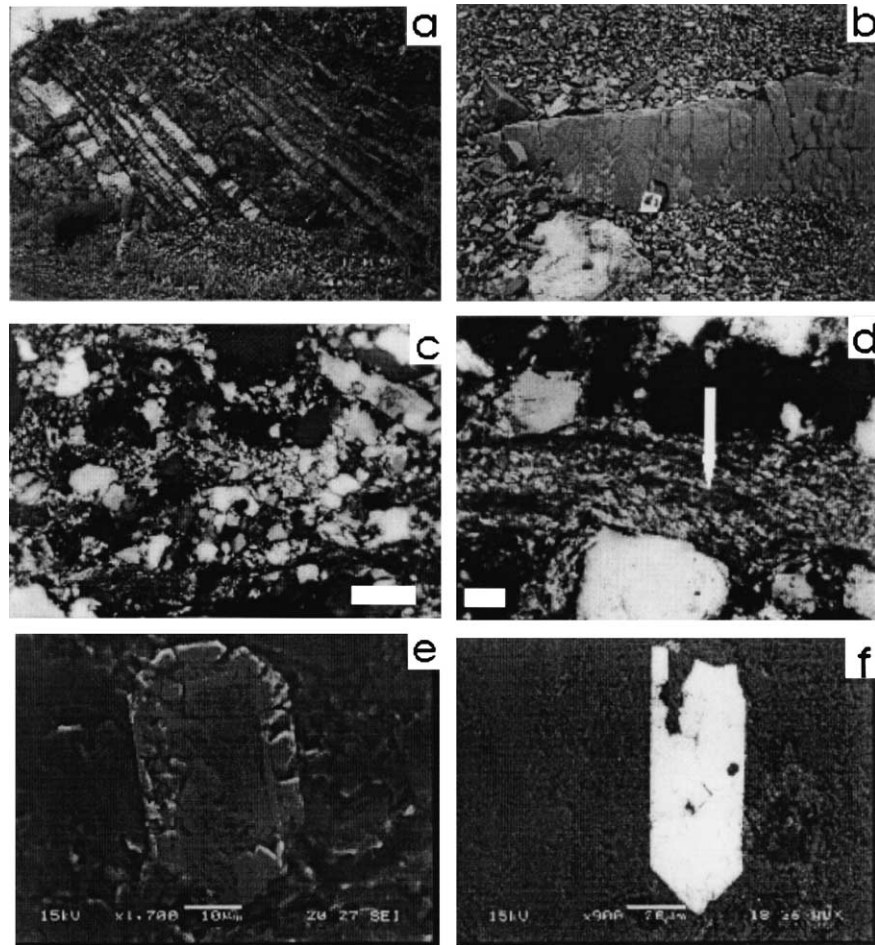


Fig. 3. (a) Panoramic view of outcrops and the upward coarsening trend. (b) Sedimentary structures with parallel and longitudinal crests. (c) Sedimentary petrography, general view of quartz-feldspar sandstone. (d) Typical low-grade metamorphic rock fragment from section C–C'. Scale 2 mm. (e) SEM image of a metamorphic zircon crystal. (f) SEM image of volcanic-type zircon crystal.

trough. [Manassero et al. \(1999\)](#) also investigate geographically dependent sedimentological variations, such as proximity to sand-feeding channels, in the unit and measure parameters such as bed thickness and sand/shale ratios. The preferred transport paths of gravity flows can be interpolated from the pattern of maximum and mean thickness of sandstone beds in the sections ([Fig. 4](#)), because sand beds are more abundant in depressions across the continental slope; sections A–A' and D–D' show a relative dominance of sandy facies over finer ones.

5. Sampling and analytical procedures

Samples were collected along four sections, shown in [Fig. 2](#) (A–A' $n = 4$; B–B' $n = 3$; C–C' $n = 23$; D–D' $n = 13$). A total of 43 sandstone and siltstone samples was analyzed under the microscope in thin section; 400 points were counted for each sample using the traditional method of [Dickinson and Suczek \(1979\)](#) and [Dickinson et al. \(1983\)](#).

For the geochemical analysis, the samples were reduced to chips of 2–4 mm, cleaned several times in distilled water, and pulverized in a tungsten carbide mill. Twenty-four whole-rock samples (sandstones, wackes, and siltstones; see [Table 1](#)) were analyzed by ACTLABS Co., Canada, for major, trace, and REE ([Tables 2–4](#)). Major elements were determined by ICP, whereas trace elements and REE were determined by ICP/MS. Sm–Nd isotopic analysis were carried out in the Geochronological Center, Universidade Federal do Rio Grande do Sul, Porto Alegre, Brazil.

Replicate analyses of samples and standards indicate that errors for major elements vary between 1 and 2%. Accuracy of the trace and REE element analyses is within 5%. The REE data were normalized relative to the chondrite values of [Taylor and McLennan \(1985\)](#).

6. Sandstone petrography and QFL diagrams

Petrographic analysis of sedimentary rocks is useful for determining provenance ([Dickinson and Suczek, 1979;](#)

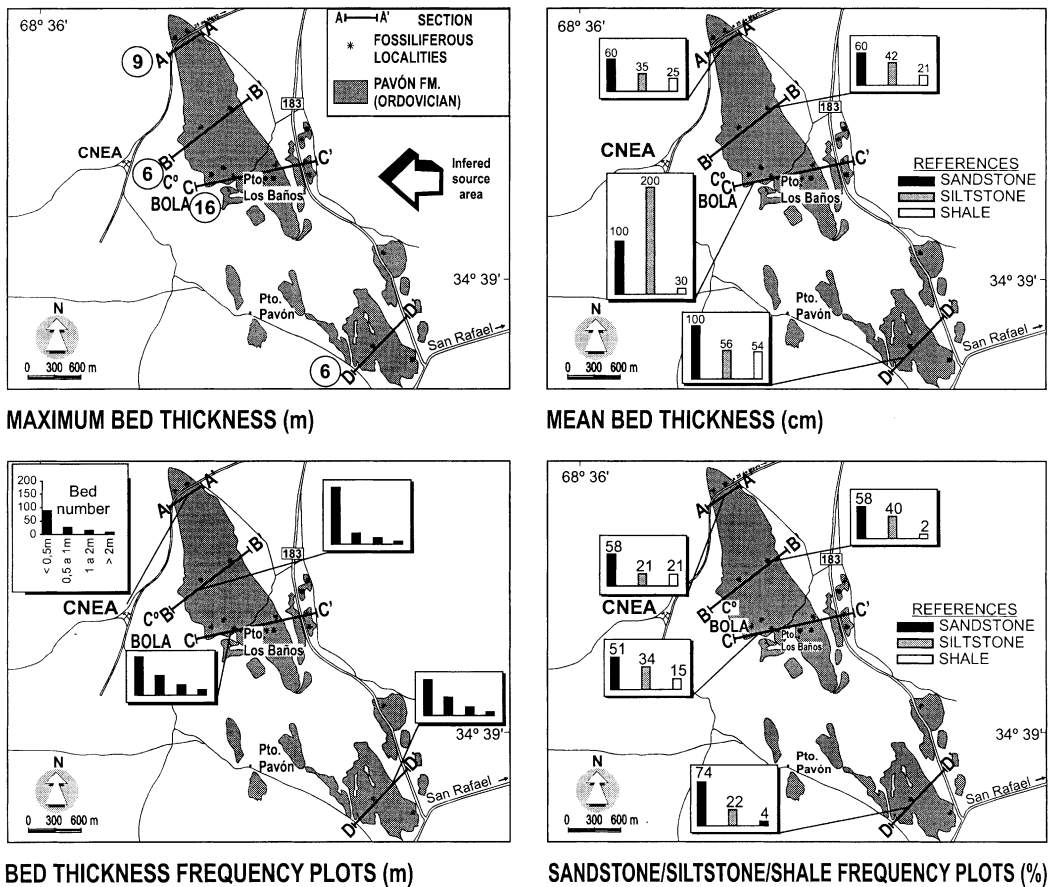


Fig. 4. Statistical data and facies distribution.

Dickinson et al., 1983). In matrix-rich rocks, microscopic methods can be enhanced by minor and trace element geochemistry, taking into account that only stable minerals are preserved during weathering and diagenesis.

Textural data (Table 1) for sandstone samples from the Pavón Formation show 15–30% matrix content, poor to moderate sorting, and medium to very fine grain sizes. The minerals recorded are quartz (monocrystalline and polycrystalline), K-feldspar, plagioclase, biotite, muscovite, opaques, tourmaline, zircon, apatite, and hematite, as well as sedimentary and metamorphic rock fragments (Fig. 3c). The most typical metamorphic rock fragments are composed of elongate quartz separated by mica plates with schistose texture (Fig. 3d). Zircon is a common heavy mineral in the sandstone samples. As shown by the SEM images (Fig. 3e and f), the zircon grains are rounded to euhedral in shape.

The analyzed samples were plotted in QFL ternary diagrams (Dickinson and Suczek, 1979; Dickinson et al., 1983), including detrital grains but excluding micas, opaques, chlorite, heavy minerals, and carbonate grains. Chert was counted as a sedimentary rock fragment (Fig. 5). Most of the sandstones are wackes (more than 15% matrix, mean 25%; Table 1) and composed of quartz, with mostly wavy extinction, feldspars, and fragments of metaquartzitic

rocks. Following Dott (1964), the sandstones could be classified as feldspathic and quartz wackes.

The sandstones show a grouping of data in both the recycled orogen and the continental block provenance fields in the QFL diagrams (Fig. 5). Our data show striking similarities to the detrital modes of some Ordovician units of the Precordillera (Loske, 1992, 1994) and suggest the same provenance. If we consider the detrital QFL modes, section by section, the percentages are as follows: A–A': $Q = 71, F = 21, L = 8$; B–B': $Q = 62, F = 29, L = 9$;

Table 1
Textural data on sandstone samples

| Sample | Matrix% | Mean size | Max. Size | Roundness | Sorting |
|--------|---------|-----------|-----------|------------|----------|
| QC1 | 30 | Fine | Medium | Angular | Poor |
| QC2 | 25 | Fine | Fine | Subangular | Poor |
| QC3 | 30 | Fine | Medium | Subrounded | Poor |
| QC4 | 20 | Fine | Medium | Subrounded | Moderate |
| QC5 | 20 | Fine | Medium | Subrounded | Moderate |
| QM3 | 15 | Very fine | Fine | Rounded | Moderate |
| QR1 | 30 | Very fine | Fine | Subangular | Moderate |
| QR3 | 25 | Fine | Medium | Subrounded | Moderate |
| QR4 | 25 | Very fine | Fine | Subangular | Moderate |
| QCN1 | 30 | Fine | Medium | Subrounded | Moderate |

Table 2

Major element geochemical data for whole-rock samples

| | QB1 | QB2 | QB3 | QB4 | QB5 | QB5r | QB6 | QM1 | QM2 | QM3 | QR1 | QR2 | QR3 |
|--|--------|--------|--------|--------|--------|--------|--------|--------|--------|--------|--------|---------|--------|
| SIO ₂ | 89.08 | 91.67 | 79.65 | 80.32 | 73.61 | 73.21 | 78.6 | 77.79 | 77.41 | 77.4 | 61.1 | 66.76 | 70.53 |
| AL ₂ O ₃ | 4.68 | 4.17 | 8.16 | 8.93 | 12.27 | 12.3 | 9.13 | 9.93 | 9.65 | 9.3 | 19.02 | 16.9 | 12.25 |
| Fe ₂ O ₃ | 0.39 | 0.47 | 4.04 | 4.51 | 5.53 | 5.54 | 4.99 | 4.51 | 4.68 | 4.44 | 7.16 | 6.15 | 5.5 |
| MnO | 0.002 | -0.001 | 0.049 | 0.009 | 0.026 | 0.026 | 0.03 | 0.033 | 0.032 | 0.024 | 0.076 | 0.064 | 0.101 |
| MgO | 0.14 | 0.15 | 1.12 | 1.01 | 1.76 | 1.76 | 1.55 | 1.55 | 1.6 | 0.46 | 1.96 | 1.6 | 2.31 |
| CaO | 0.04 | 0.02 | 0.93 | 0.13 | 0.19 | 0.19 | 0.19 | 0.36 | 0.21 | 0.79 | 0.24 | 0.19 | 1.39 |
| Na ₂ O | 0.52 | 0.02 | 0.79 | -0.01 | -0.01 | -0.01 | 0.87 | -0.01 | 0.87 | 0.74 | 0.91 | 0.72 | 1.98 |
| K ₂ O | 0.84 | 1.12 | 1.48 | 1.72 | 2.29 | 2.33 | 1.54 | 1.77 | 1.81 | 1.78 | 3.72 | 3.41 | 1.86 |
| TiO ₂ | 0.537 | 0.636 | 0.814 | 0.906 | 1.088 | 1.096 | 0.9 | 0.956 | 0.869 | 0.964 | 1.167 | 1.213 | 1.015 |
| P ₂ O ₅ | 0.04 | 0.05 | 0.1 | 0.1 | 0.15 | 0.14 | 0.12 | 0.14 | 0.14 | 0.13 | 0.15 | 0.16 | 0.15 |
| LOI | 3.79 | 2.03 | 3.01 | 2.64 | 3.57 | 3.57 | 2.23 | 3.23 | 2.45 | 3.65 | 3.56 | 3.12 | 3.28 |
| TOTAL | 100.05 | 100.33 | 100.15 | 100.25 | 100.46 | 100.14 | 100.15 | 100.28 | 99.74 | 99.68 | 99.05 | 100.29 | 100.36 |
| CIW | 89.31 | 99.05 | 82.59 | | | | 89.6 | | 89.93 | 85.87 | 94.3 | 94.89 | 78.43 |
| CIA | 76.97 | 78.24 | 71.83 | | | | 77.83 | | 76.95 | 73.75 | 79.61 | 79.64 | 70.08 |
| AL ₂ O ₃ /SiO ₂ | 0.05 | 0.05 | 0.10 | 0.11 | 0.17 | 0.17 | 0.12 | 0.13 | 0.12 | 0.12 | 0.31 | 0.25 | 0.17 |
| K ₂ O/Na ₂ O | 1.62 | 56.00 | 1.87 | | | | 1.77 | | 2.08 | 2.41 | 4.09 | 4.74 | 0.94 |
| FE ₂ O ₃ /MgO | 2.79 | 3.13 | 3.61 | 4.47 | 3.14 | 3.15 | 3.22 | 2.91 | 2.93 | 9.65 | 3.65 | 3.84 | 2.38 |
| QR4 | QR4 | QCN1 | PV1 | PV5 | PV8 | PV9 | PV10 | PV11 | PV13 | PV11' | PV12 | Average | |
| SIO ₂ | 69.4 | 70.97 | 74.68 | 84.31 | 80.59 | 74.66 | 71.61 | 75.07 | 84.89 | 71.68 | 75.14 | 76.26 | |
| AL ₂ O ₃ | 11.45 | 10.52 | 9.89 | 6.54 | 8.83 | 11.02 | 12.41 | 11.01 | 7.39 | 12.66 | 11.71 | 10.42 | |
| Fe ₂ O ₃ | 5.86 | 6.68 | 9.03 | 5.08 | 2.77 | 4.87 | 5.95 | 5.79 | 2.61 | 5.96 | 5.23 | 4.91 | |
| MnO | 0.065 | 0.062 | 0.002 | -0.001 | 0.013 | 0.043 | 0.041 | 0.043 | 0.006 | 0.046 | 0.014 | 0.04 | |
| MgO | 2.7 | 3.08 | 0.34 | 0.2 | 0.68 | 0.85 | 1.78 | 1.9 | 0.48 | 2.07 | 0.82 | 1.33 | |
| CaO | 1.75 | 1.1 | 0.04 | 0.05 | 0.04 | 0.66 | 0.62 | 0.27 | 0.08 | 0.44 | 0.22 | 0.42 | |
| Na ₂ O | 2.07 | 1.42 | 0.13 | 0.08 | 0.08 | 1.07 | 1.13 | 0.06 | 0.06 | 1.1 | 0.09 | 0.74 | |
| K ₂ O | 1.83 | 1.18 | 2.22 | 1.25 | 1.39 | 1.83 | 1.9 | 1.53 | 1.18 | 2.07 | 1.99 | 1.84 | |
| TiO ₂ | 0.914 | 1.591 | 1.113 | 0.687 | 0.817 | 1.18 | 1.282 | 1.124 | 0.716 | 1.161 | 0.97 | 0.99 | |
| P ₂ O ₅ | 0.14 | 0.26 | 0.06 | 0.05 | 0.13 | 0.16 | 0.2 | 0.16 | 0.43 | 0.14 | 0.13 | 0.14 | |
| LOI | 3.68 | 3.36 | 2.93 | 2.14 | 3.25 | 3.92 | 3.54 | 3.52 | 2.65 | 3.15 | 3.69 | 3.17 | |
| TOTAL | 99.87 | 100.22 | 100.42 | 100.38 | 98.57 | 100.25 | 100.45 | 100.47 | 100.49 | 100.47 | 100.01 | 100.11 | |
| CIW | 74.98 | 80.67 | 98.31 | 98.05 | 98.66 | 86.43 | 87.64 | 97.09 | 98.14 | 89.15 | 97.42 | 90.53 | |
| CIA | 66.96 | 73.98 | 80.54 | 82.58 | 85.40 | 78.58 | 77.27 | 85.55 | 84.85 | 77.81 | 83.58 | 78.10 | |
| AL ₂ O ₃ /SiO ₂ | 0.16 | 0.15 | 0.13 | 0.08 | 0.11 | 0.15 | 0.17 | 0.15 | 0.09 | 0.18 | 0.16 | 0.14 | |
| K ₂ O/Na ₂ O | 0.88 | 0.83 | 17.08 | 15.63 | 17.38 | 1.71 | 1.68 | 25.50 | 19.67 | 1.88 | 22.11 | 9.99 | |
| FE ₂ O ₃ /MgO | 2.17 | 2.17 | 26.56 | 25.40 | 4.07 | 5.73 | 3.34 | 3.05 | 5.44 | 2.88 | 6.38 | 5.67 | |

C–C': $Q = 70, F = 21, L = 9$; and D–D': $Q = 79, F = 10, L = 11$. The average is therefore $Q = 70, F = 10$, and $L = 11$.

Much of the scatter in the data results from differences in the populations of quartz and feldspar grains. Although they show considerable dispersion, we can infer an uplifted continental fragment as a likely source area. Paleocurrent data suggest that this exposed land was located east of the study area (Manassero et al., 1999).

7. Geochemistry

7.1. Sediment weathering, recycling, and sources

Alteration of rocks during weathering results in depletion of alkalis and alkaline earths and preferential enrichment of Al₂O₃. Weathering effects can be evaluated in terms of the molecular percentage of the oxide components, using the formulae chemical index of

weathering (CIW = Al₂O₃/(Al₂O₃ + CaO* + Na₂O; cf. Harnois, 1988) or chemical index of alteration (CIA = Al₂O₃/(Al₂O₃ + CaO* + Na₂O + K₂O; cf. Nesbitt and Young, 1982). Variations in these two ratios reflect variations in mineralogical composition. The average CIA value of the Pavón Formation (Table 2) is 78.10, with SiO₂ contents ranging from 66 to 91% (Fig. 6a). Another way to represent the CIA is in the triangle depicted in Fig. 6b, in which the samples plot mostly in the upper part nearest the illite composition, which indicates a high degree of alteration. The CIW values are also high, as shown in Fig. 6c. Most of the Pavón Formation sedimentary rocks have low CaO (average 0.42 wt.%) and relatively high K₂O (average 1.84 wt.%), whereas the Fe₂O₃ and MgO contents are similar to those of the average upper continental crust. SiO₂ contents reflect the intermediate to quartz-rich nature of the samples (Table 2).

The chemical composition of sedimentary rocks is also influenced by hydraulic sorting; thus, the hydraulic concentration of weathering-resistant phases such as zircon, Cr-spinel, monazite, and apatite may produce irregular

Table 3

Trace element geochemical data for whole-rock samples

| | QB1 | QB2 | QB3 | QB4 | QB5 | QB5r | QB6 | QM1 | QM2 | QM3 | QR1 | QR2 | QR3 |
|----|------|------|------|------|------|------|------|------|------|-------|------|---------|------|
| Sc | 8 | 9 | 10 | 13 | 19 | 17 | 14 | 16 | 14 | 14 | 19 | 20 | 18 |
| Be | 1 | -1 | -1 | 1 | 2 | 1 | 1 | 1 | 1 | 1 | 2 | 2 | 2 |
| V | 66 | 68 | 74 | 101 | 136 | 125 | 109 | 101 | 91 | 95 | 144 | 136 | 111 |
| Cr | 65 | 69 | 111 | 111 | 134 | 123 | 111 | 141 | 139 | 137 | 119 | 114 | 283 |
| Co | 33 | 74 | 41 | 46 | 18 | 18 | 37 | 37 | 34 | 55 | 27 | 27 | 27 |
| Ni | -20 | -20 | 52 | 68 | 33 | 39 | 58 | 47 | 59 | 98 | 31 | 56 | 467 |
| Cu | -10 | -10 | -10 | -10 | 31 | 32 | -10 | -10 | 22 | -10 | 44 | 39 | 24 |
| Zn | -30 | -30 | 61 | 80 | 113 | 112 | 171 | 100 | 316 | 102 | 103 | 95 | 72 |
| Ga | 6 | 7 | 11 | 12 | 17 | 16 | 12 | 14 | 14 | 14 | 26 | 24 | 17 |
| Ge | 1.3 | 1.6 | 1.3 | 1.8 | 1.7 | 1.7 | 1.7 | 1.7 | 1.7 | 1.7 | 2.1 | 1.9 | 1.6 |
| As | 13 | 6 | -5 | 8 | 12 | 12 | 11 | -5 | -5 | 10 | -5 | -5 | 45 |
| Rb | 34 | 43 | 56 | 65 | 87 | 82 | 56 | 67 | 71 | 69 | 189 | 168 | 74 |
| Sr | 43 | 58 | 73 | 55 | 30 | 29 | 49 | 23 | 48 | 68 | 95 | 73 | 87 |
| Y | 25.8 | 29.8 | 29.2 | 36.3 | 35.5 | 33.6 | 31.7 | 34.8 | 32.6 | 32 | 39.1 | 34.8 | 33.3 |
| Zr | 321 | 324 | 288 | 310 | 326 | 307 | 316 | 305 | 263 | 333 | 222 | 245 | 303 |
| Nb | 6.7 | 8.6 | 11.6 | 13.6 | 17.2 | 16.4 | 12 | 14.6 | 12.9 | 15.4 | 23.1 | 24.1 | 19.7 |
| Mo | -2 | -2 | -2 | -2 | -2 | -2 | -2 | -2 | -2 | -2 | -2 | -2 | -2 |
| Ag | -0.5 | -0.5 | -0.5 | -0.5 | -0.5 | -0.5 | -0.5 | -0.5 | -0.5 | -0.5 | -0.5 | -0.5 | -0.5 |
| In | -0.1 | -0.1 | -0.1 | -0.1 | -0.1 | -0.1 | -0.1 | -0.1 | -0.1 | -0.1 | -0.1 | -0.1 | -0.1 |
| Sn | 1 | 1 | 2 | 2 | 3 | 2 | 2 | 3 | 2 | 2 | 4 | 4 | 2 |
| Sb | 2.5 | 0.6 | 0.3 | 0.6 | 3.1 | 3.3 | 0.8 | 1.8 | 1 | 3.3 | 1.4 | 1.2 | 0.5 |
| Cs | 2.1 | 2 | 2.4 | 2.5 | 4.3 | 4.1 | 2.2 | 2.7 | 2.8 | 2.9 | 9.2 | 7.2 | 3.3 |
| Ba | 744 | 1620 | 744 | 590 | 479 | 480 | 265 | 293 | 324 | 411 | 651 | 501 | 456 |
| Hf | 7.8 | 8 | 8.1 | 8.6 | 8.6 | 8.6 | 8.6 | 8.6 | 7.4 | 9.1 | 6.8 | 7.4 | 8.6 |
| Ta | 1.88 | 4.87 | 3.59 | 4.47 | 2.21 | 2.19 | 3.05 | 3.22 | 3.19 | 4.43 | 2.23 | 2.44 | 3.11 |
| W | 233 | 749 | 518 | 638 | 156 | 148 | 368 | 410 | 393 | 637 | 69.6 | 91.8 | 308 |
| Tl | 0.57 | 0.69 | 0.49 | 0.44 | 0.45 | 0.48 | 0.34 | 0.33 | 0.41 | 0.43 | 0.88 | 0.74 | 0.33 |
| Pb | -5 | -5 | 5 | -5 | 8 | -5 | 7 | -5 | 9 | 8 | 16 | 13 | 12 |
| Bi | -0.1 | 0.1 | -0.1 | 0.1 | -0.1 | -0.1 | -0.1 | 0.1 | -0.1 | 0.2 | 0.3 | 0.3 | 0.1 |
| Th | 6.35 | 5.77 | 7.38 | 8.28 | 9.86 | 10 | 8.11 | 8.61 | 8.75 | 8.75 | 15.7 | 14.7 | 9.93 |
| U | 4.03 | 5.67 | 1.79 | 3.54 | 3.88 | 3.82 | 1.9 | 3.29 | 2.82 | 2.98 | 3.75 | 2.81 | 3.06 |
| | QR4 | QCN1 | PV1 | PV5 | PV8 | PV9 | PV10 | PV11 | PV13 | PV11' | PV12 | Average | |
| Sc | 15 | 19 | 12 | 9 | 10 | 14 | 15 | 14 | 8 | 15 | 14 | 14.0 | |
| Be | 2 | 1 | 2 | 1 | 1 | 2 | 2 | 2 | 1 | 2 | 1 | 1.5 | |
| V | 96 | 145 | 117 | 74 | 68 | 104 | 111 | 164 | 79 | 106 | 272 | 112.2 | |
| Cr | 127 | 292 | 116 | 84 | 110 | 159 | 166 | 179 | 112 | 167 | 165 | 138.9 | |
| Co | 33 | 45 | 12 | 26 | 35 | 21 | 24 | 36 | 25 | 27 | 17 | 32.3 | |
| Ni | 48 | 64 | -20 | 22 | 38 | 32 | 33 | 89 | 43 | 54 | 70 | 71.5 | |
| Cu | 21 | 19 | -10 | 19 | 23 | 39 | 38 | 24 | 13 | 47 | 17 | 28.3 | |
| Zn | 61 | 81 | -30 | -30 | -30 | -30 | 83 | 222 | 72 | 33 | 44 | 106.7 | |
| Ga | 14 | 14 | 16 | 10 | 10 | 15 | 18 | 15 | 10 | 18 | 19 | 14.5 | |
| Ge | 1.2 | 1.5 | 1.7 | 1.6 | 1.1 | 1.6 | 1.8 | 1.9 | 1.5 | 1.6 | 3.3 | 1.7 | |
| As | -5 | -5 | 8 | 9 | -5 | -5 | -5 | 16 | 15 | -5 | 56 | 17.0 | |
| Rb | 68 | 44 | 96 | 55 | 55 | 71 | 78 | 62 | 58 | 85 | 127 | 77.5 | |
| Sr | 106 | 84 | 47 | 167 | 55 | 75 | 70 | 32 | 157 | 57 | 188 | 73.7 | |
| Y | 28.7 | 36.5 | 35.9 | 25 | 27.1 | 29 | 35.7 | 35.6 | 26.5 | 38.3 | 48.5 | 33.1 | |
| Zr | 245 | 399 | 311 | 271 | 239 | 292 | 300 | 298 | 287 | 356 | 307 | 298.7 | |
| Nb | 16 | 23.1 | 22.3 | 11.1 | 12.1 | 22 | 25.4 | 21.1 | 13.5 | 23.8 | 20.1 | 16.9 | |
| Mo | -2 | -2 | 3 | 8 | -2 | -2 | -2 | 3 | 5 | -2 | 24 | 8.6 | |
| Ag | -0.5 | -0.5 | -0.5 | -0.5 | -0.5 | -0.5 | -0.5 | -0.5 | -0.5 | -0.5 | -0.5 | -0.5 | |
| In | -0.1 | -0.1 | -0.1 | -0.1 | -0.1 | -0.1 | -0.1 | -0.1 | -0.1 | -0.1 | -0.1 | -0.1 | |
| Sn | 2 | 2 | 3 | 1 | 1 | 2 | 3 | 2 | 2 | 3 | 3 | 2.3 | |
| Sb | 0.4 | 0.5 | 2.7 | 2 | 0.6 | 0.8 | 0.7 | 1.1 | 0.8 | 1.2 | 14.2 | 1.9 | |
| Cs | 2.6 | 1.8 | 5.2 | 3.3 | 1.8 | 2.9 | 3.2 | 2.6 | 4.1 | 2.8 | 12.5 | 3.8 | |
| Ba | 388 | 229 | 2940 | 1690 | 480 | 298 | 336 | 315 | 517 | 377 | 598 | 655.3 | |
| Hf | 6.8 | 10.4 | 9.6 | 7.5 | 6.9 | 8.6 | 9.1 | 8.9 | 8.3 | 10.8 | 8.3 | 8.4 | |
| Ta | 2.77 | 3.48 | 1.96 | 2.5 | 4.08 | 2.21 | 2.45 | 2.35 | 1.97 | 2.17 | 2.02 | 2.9 | |
| W | 305 | 324 | 61 | 339 | 450 | 119 | 136 | 181 | 213 | 103 | 132 | 295.1 | |
| Tl | 0.3 | 0.21 | 3.74 | 1.62 | 0.22 | 0.24 | 0.66 | 0.52 | 0.45 | 0.3 | 0.18 | 0.6 | |
| Pb | 8 | 7 | 6 | -5 | -5 | 9 | 9 | -5 | -5 | -5 | -5 | 9.0 | |
| Bi | -0.1 | -0.1 | 0.3 | 0.2 | -0.1 | -0.1 | 0.4 | 0.3 | 0.1 | 0.1 | -0.1 | 0.2 | |
| Th | 8.52 | 8.2 | 10.7 | 7.45 | 7.55 | 9.31 | 10.4 | 9.15 | 6.94 | 12 | 10.9 | 9.3 | |
| U | 1.97 | 2.32 | 3.44 | 4.66 | 3.6 | 2.37 | 2.64 | 3.23 | 2.17 | 2.66 | 4.22 | 3.2 | |

Table 4

Rare earth element data for whole-rock samples

| | QB1 | QB2 | QB3 | QB4 | QB5 | QB5r | QB6 | QM1 | QM2 | QM3 | QR1 | QR2 | QR3 | |
|-----|-------|-------|-------|-------|-------|-------|-------|-------|-------|-------|---------|-------|-------|----|
| | La | Ce | Pr | Nd | Sm | Eu | Gd | Tb | Dy | Ho | Er | Tm | Yb | Lu |
| La | 18 | 22 | 26.1 | 30.2 | 38.1 | 38.2 | 27.9 | 29.3 | 31.8 | 32.1 | 54.2 | 49.7 | 39.9 | |
| Ce | 39 | 49.2 | 58.6 | 67.4 | 84.3 | 82 | 62.3 | 63.8 | 69.4 | 71.9 | 117 | 104 | 86 | |
| Pr | 4 | 5.65 | 6.49 | 7.41 | 9.54 | 9.23 | 6.99 | 7.17 | 7.82 | 8.09 | 12.8 | 11.4 | 9.71 | |
| Nd | 13.8 | 22.4 | 25.2 | 28.5 | 36.3 | 35.3 | 27.1 | 27.8 | 31 | 30.6 | 47.2 | 42.6 | 36.7 | |
| Sm | 2.34 | 4.83 | 5.59 | 6.13 | 7.55 | 7.31 | 5.84 | 6.03 | 6.84 | 6.44 | 9.51 | 8.33 | 7.65 | |
| Eu | 0.399 | 0.818 | 1.11 | 1.26 | 1.53 | 1.44 | 1.28 | 1.21 | 1.36 | 1.33 | 1.86 | 1.68 | 1.65 | |
| Gd | 2.9 | 4.62 | 5.05 | 5.72 | 6.59 | 6.48 | 5.56 | 5.55 | 6.2 | 5.62 | 7.51 | 7.2 | 6.77 | |
| Tb | 0.62 | 0.83 | 0.97 | 1.09 | 1.19 | 1.17 | 1.04 | 0.99 | 1.11 | 1.01 | 1.31 | 1.25 | 1.18 | |
| Dy | 4.27 | 5.12 | 5.72 | 6.62 | 7.06 | 6.86 | 6.19 | 5.9 | 6.51 | 6.15 | 7.7 | 7.02 | 6.85 | |
| Ho | 0.96 | 1.07 | 1.2 | 1.41 | 1.48 | 1.42 | 1.31 | 1.25 | 1.34 | 1.29 | 1.6 | 1.47 | 1.4 | |
| Er | 2.98 | 3.27 | 3.46 | 4.12 | 4.32 | 4.32 | 3.89 | 3.82 | 3.83 | 3.76 | 4.78 | 4.43 | 4.14 | |
| Tm | 0.446 | 0.516 | 0.56 | 0.643 | 0.65 | 0.689 | 0.626 | 0.613 | 0.618 | 0.593 | 0.739 | 0.708 | 0.657 | |
| Yb | 2.98 | 3.33 | 3.57 | 4.12 | 4.29 | 4.29 | 3.74 | 3.72 | 3.67 | 3.79 | 4.66 | 4.44 | 4.01 | |
| Lu | 0.476 | 0.486 | 0.519 | 0.631 | 0.612 | 0.604 | 0.545 | 0.569 | 0.537 | 0.577 | 0.656 | 0.669 | 0.587 | |
| QR4 | QCN1 | PV1 | PV5 | PV8 | PV9 | PV10 | PV11 | PV13 | PV11' | PV12 | Average | | | |

| | La | Ce | Pr | Nd | Sm | Eu | Gd | Tb | Dy | Ho | Er | Tm | Yb | Lu |
|----|-------|-------|-------|-------|-------|-------|-------|-------|-------|-------|-------|-------|----|----|
| La | 33.5 | 37.6 | 34.3 | 22.5 | 23.6 | 24.6 | 35.2 | 29.4 | 21.5 | 36.6 | 40.6 | 32.37 | | |
| Ce | 70.8 | 80.4 | 79.3 | 47.9 | 53.7 | 65.8 | 80.9 | 67 | 49.4 | 83.2 | 84 | 71.55 | | |
| Pr | 8.05 | 9.46 | 8.2 | 4.51 | 5.88 | 6.5 | 8.48 | 7.24 | 5.46 | 8.8 | 9.84 | 7.86 | | |
| Nd | 30.7 | 37.9 | 33.4 | 16.5 | 24 | 27 | 35.9 | 30.3 | 22.7 | 35.9 | 40.6 | 30.81 | | |
| Sm | 6.23 | 8.41 | 6.59 | 3.17 | 4.87 | 5.94 | 7.38 | 6.53 | 5.09 | 7.56 | 8.24 | 6.43 | | |
| Eu | 1.37 | 1.97 | 1.1 | 0.63 | 0.99 | 1.42 | 1.71 | 1.43 | 1.01 | 1.6 | 1.75 | 1.33 | | |
| Gd | 5.75 | 7.35 | 6.57 | 4.15 | 5.01 | 5.99 | 7.28 | 6.63 | 4.98 | 7.39 | 8.17 | 6.04 | | |
| Tb | 0.98 | 1.21 | 1.07 | 0.73 | 0.86 | 0.99 | 1.23 | 1.14 | 0.83 | 1.23 | 1.39 | 1.06 | | |
| Dy | 5.56 | 6.69 | 6.59 | 4.41 | 5.14 | 5.93 | 7.18 | 6.91 | 4.95 | 7.5 | 7.79 | 6.28 | | |
| Ho | 1.17 | 1.36 | 1.39 | 0.96 | 1.05 | 1.21 | 1.46 | 1.4 | 0.99 | 1.57 | 1.58 | 1.31 | | |
| Er | 3.43 | 3.9 | 4.12 | 2.81 | 2.94 | 3.52 | 4.31 | 3.98 | 2.95 | 4.53 | 4.94 | 3.86 | | |
| Tm | 0.537 | 0.62 | 0.64 | 0.436 | 0.454 | 0.527 | 0.647 | 0.585 | 0.449 | 0.7 | 0.711 | 0.60 | | |
| Yb | 3.25 | 3.68 | 4.11 | 3.03 | 3.04 | 3.46 | 4.3 | 3.96 | 2.95 | 4.7 | 4.44 | 3.81 | | |
| Lu | 0.484 | 0.529 | 0.611 | 0.448 | 0.437 | 0.519 | 0.616 | 0.587 | 0.435 | 0.686 | 0.675 | 0.56 | | |

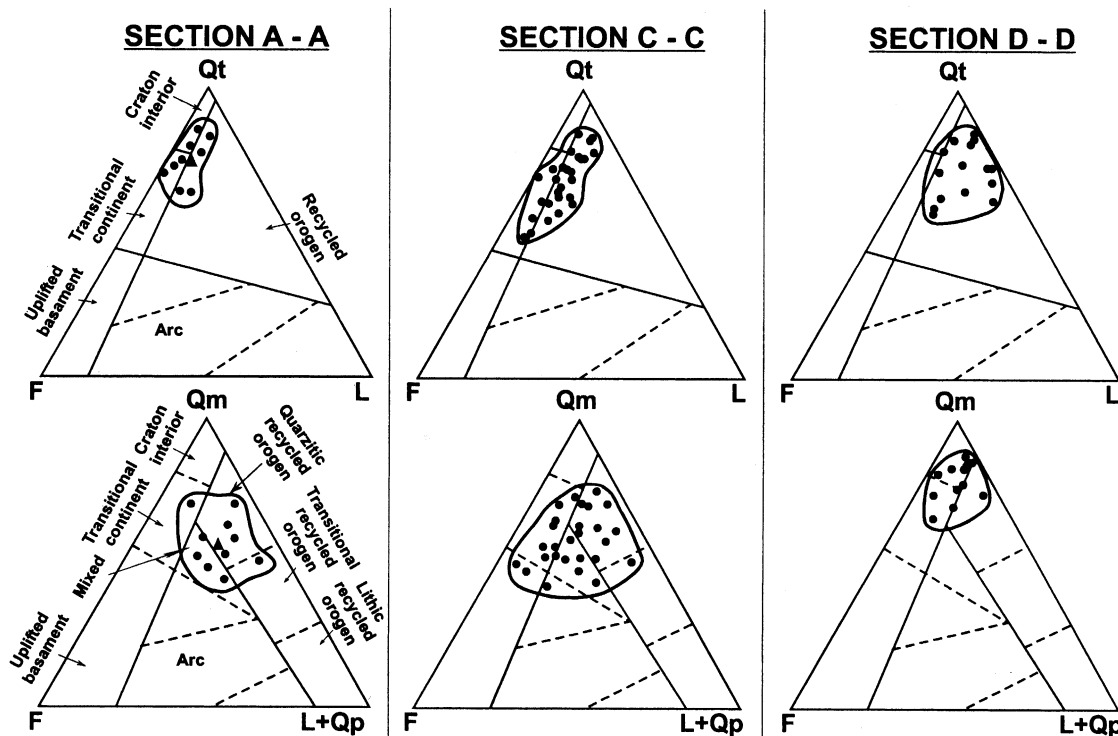


Fig. 5. Ternary diagrams for provenance following Dickinson and Suczek (1979) and Dickinson et al. (1983) for three sections of the Pavón Formation sandstones.

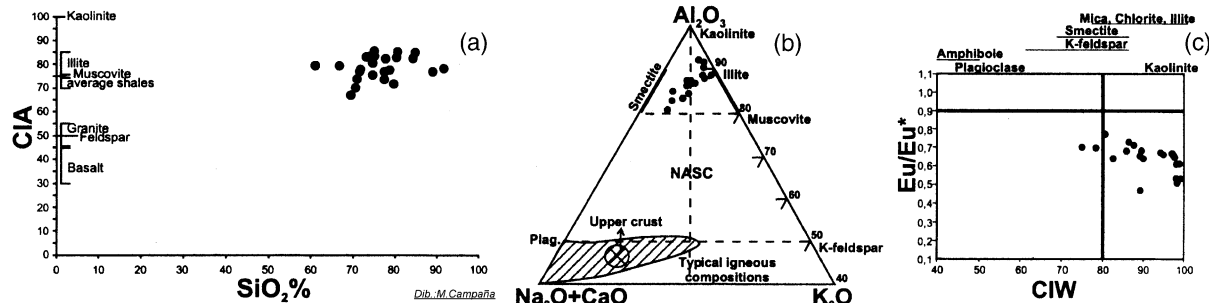


Fig. 6. (a) CIA versus SiO_2 , after Nesbitt and Young (1982). (b) CIA as an indicator of the degree of alteration. The samples plot mostly in the upper part of the triangle, near illite composition. NASC = North American shales composition. (c) CIW (Harnois, 1988) versus Eu/Eu^* . The average value of CIW suggests high degrees of weathering of the source.

chemical variations in some trace elements (Cullers et al., 1979; Mass and McCulloch, 1991). Enrichment of Zr is shown by high Zr/Sc ratios (Fig. 7a) and Zr/Sc versus SiO_2 (Fig. 7b), which indicate significant reworking and/or selective sorting. Th and Sc are incompatible and compatible, respectively, in igneous differentiation processes, so Th/Sc indicates the degree of igneous differentiation (McLennan et al., 1993). The Pavón Formation samples have relatively moderate Th/Sc ratios (average 0.78) and therefore reflect input from fairly evolved crustal igneous sources. Th/Sc ratios less than 0.8 are typically found in mature sands deposited at passive margins. Hydraulic sorting also may be evaluated in plots of Gd/Yb versus La/Sm , in which the Pavón Formation data show significant scatter (Fig. 7c).

Fig. 8a is a provenance discrimination diagram based on K/Rb ratios (Floyd and Leveridge, 1987; Floyd et al., 1990), in which the Pavón Formation samples are compatible with derivation from silicic acid and intermediate magmatic precursors, as proposed by Manassero et al. (1999). K and Rb are considered relatively mobile during diagenesis and low-grade metamorphism, but the same conclusion is suggested by the discriminant scheme of Winchester and Floyd (1977), which is based on the immobile trace elements ratios Zr/TiO_2 and Nb/Y (Fig. 8b). The Pavón Formation samples have Nb/Y ratios between 0.26 and 0.76 (average 0.51) and Zr/TiO_2 ratios between 0.03 and 0.10 (average 0.053), which indicate a rhyodacitic protolith, though four samples have trachyandesitic or andesitic characteristics.

7.2. Provenance and tectonic setting

Roser and Korsch (1986) use major element patterns to discriminate tectonic settings. In the diagram shown in Fig. 9a, most of the Pavón Formation samples fall into the passive margin field, except three that plot in the active continental margin field. A similar pattern was found for Ordovician siliciclastic rocks from the Precordillera (Loske, 1992). The patterns may be compared to those of recent deep-sea turbidites derived and deposited at passive margin.

The discriminant functions of Roser and Korsch (1988) use Al_2O_3 , TiO_2 , $\text{Fe}_2\text{O}_3\text{T}$, MgO , CaO , Na_2O , and K_2O contents as variables. These were designed to discriminate among four sedimentary provenances: mafic, P1: ocean island arc; intermediate, P2: mature island arc; felsic, P3: active continental margin; and recycled, P4: granitic-gneissic or sedimentary source. In this diagram (Fig. 9b), the majority of the Pavón Formation samples plot on the P4 field of recycled continental sources associated with a passive continental margin, intracratonic sedimentary basins, and recycled orogenic provinces. As noted previously, provenance discrimination diagrams based only on major elements are unreliable because of the mobilization of these components during weathering and alteration.

Certain trace elements and REE are most suitable for the determination of provenance and tectonic setting (e.g. Bhatia, 1983; Taylor and McLennan, 1985; Bhatia and

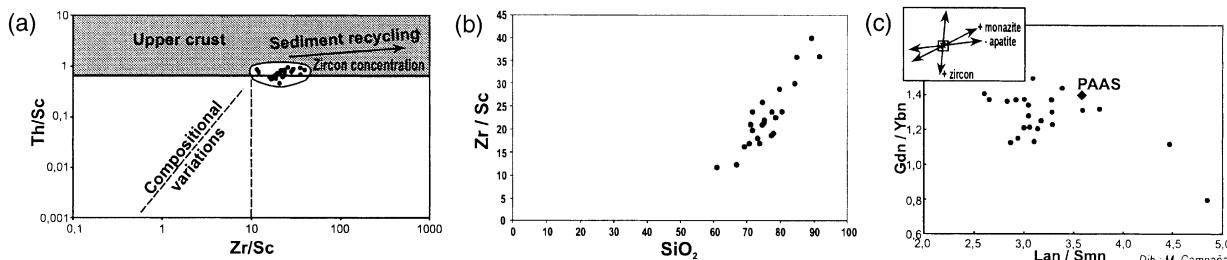


Fig. 7. (a) Th/Sc versus Zr/Sc diagram after McLennan et al. (1993), reflecting reworking and upper crust input. (b) Plot of Zr/Sc versus SiO_2 trend. (c) $\text{Gd}_{\text{P}}/\text{Yb}_{\text{N}}$ versus $\text{La}_{\text{P}}/\text{Sm}_{\text{N}}$ showing scattered correlation for Pavón Formation sandstones. The PAAS average is shown for reference (Taylor and McLennan, 1985). The effect of heavy mineral sorting is explained in the inset.

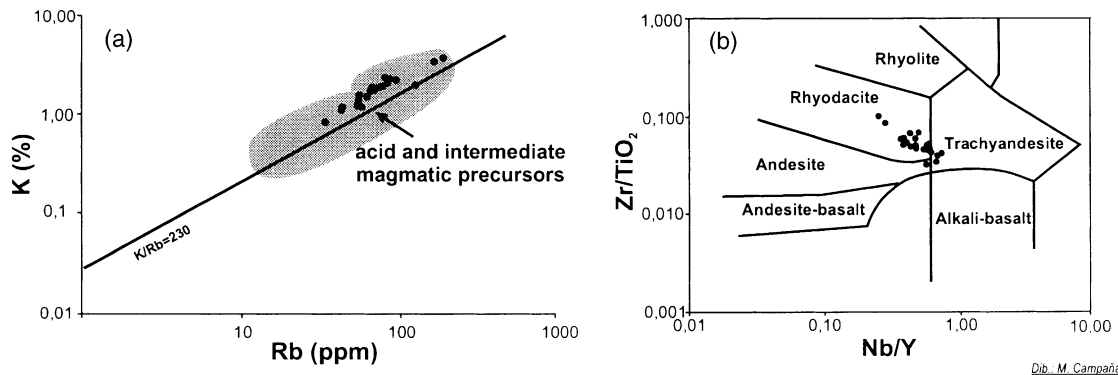


Fig. 8. (a) Rb–K diagram showing the correspondence of Pavón Formation samples to silicic and intermediate magmatic precursors (Floyd et al., 1990). (b) Winchester and Floyd (1977) diagram; most Pavón Formation samples follow a rhyodacite to trachyandesite compositional trend, but one sample has an andesite composition.

Crook, 1986) because of their relatively low mobility during sedimentary processes and their low residence time in seawater. These elements are generally thought to be quantitatively transported into clastic sedimentary rocks after weathering, and thus, they may reflect the signature of parent materials. However, possible fractionation of REE during diagenesis or low-grade metamorphism has been observed (Milodowski and Zalasiewicz, 1991; Bock et al., 1994).

The studied rocks show enrichment in Cr, with abundances mostly between 65 and 179 ppm, compared with the average upper continental crust of approximately 80 ppm. Two samples have even higher concentrations (283 and 292 ppm), the first with a higher Ni content (467 ppm). These data are not compatible with typical upper continental crust rocks but may reflect mixed sources. The Pavón Formation samples have Cr/V values between 0.5 and 0.83 with Y/Ni less than 1.3 (Fig. 10a). Both the post-Archean Australian average shale (PAAS) and the upper crust average compositions (UC) fall below these values. The relative abundances of V, Cr,

Ni, Ti, and Sc tend to indicate some mafic input, but there is no evidence for an ophiolitic derivation in the Pavón Formation.

Trace element ratios such as La/Th, La/Sc, Ti/Zr, and the Eu anomaly (Eu/Eu*) have been used to discriminate turbidites from different tectonic settings (Bhatia and Crook, 1986; Floyd and Leveridge, 1987). In the double ternary plot of Th–Sc–Zr/10 and La–Th–Sc, the Pavón Formation samples fall in the field of continental island arcs (Fig. 11), and the expected Nb negative anomaly occurs. This interpretation must be made cautiously, because specific tectonic settings do not necessarily produce rocks with unique geochemical signatures (McLennan et al., 1990; Bahlburg, 1998), and the continental crust itself has an arc-like composition (Bock et al., 2000).

The chondrite-normalized REE plots of the Pavón samples show moderate enrichment of LREE (La–Sm) relative to HREE (Gd–Yb), which have a flat pattern (Fig. 12a). This is similar to REE patterns of upper crustal rocks (McLennan, 1989). All samples of the Pavón

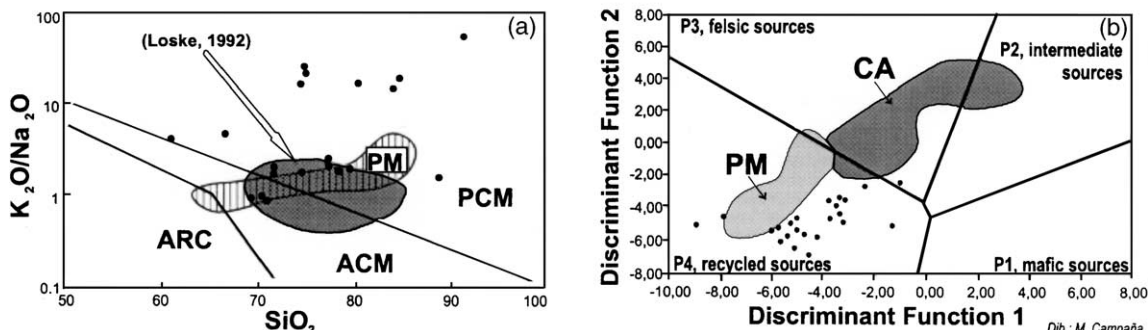


Fig. 9. (a) K_2O/Na_2O versus SiO_2 plot with discrimination fields after Roser and Korsch (1986). ARC = island arc; ACM = active continental margin; PCM = passive continental margin. Ordovician siliciclastics from the Precordillera are shown in grey (Loske, 1992). PM = recent deep-sea turbidites derived from and deposited at passive margin. Pavón Formation samples fall in PCM and ACM. (b) Discriminant diagram after Roser and Korsch (1988); the samples plot in the field P4, quartz-rich sediments of mature continental provenance, associated with a continental passive margin, intracratonic basins, or recycled orogenic provinces.

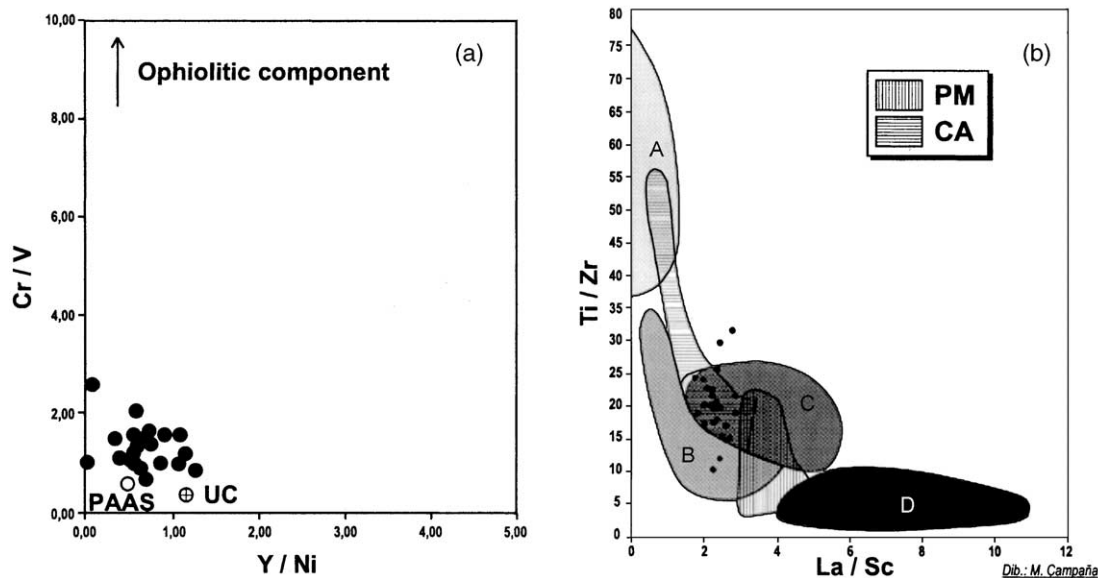


Fig. 10. (a) Plot of Cr/V versus Y/Ni. PAAS = post-Archean Australian shales; UC = upper crust. The arrow points toward an ophiolitic end member composition with extremely high Cr/V ratios. (b) La/Sc versus Ti/Zr discriminant plot of tectonic setting (Bhatia and Crook, 1986). A = oceanic island arc; B = continental island arc; C = active continental margin; D = passive margin; PM = recent deep-sea turbidites derived from and deposited at a passive margin; CA = recent deep-sea turbidites derived from and deposited at a continental arc margin (data from McLennan et al., 1990).

sandstones have Eu/Eu* values less than 1 (0.47–0.77). The sample with the most marked negative Eu anomaly (QB1) has high silica and high Zr contents (the latter indicating heavy minerals concentration; see Table 3). Comparison with the REE pattern of the PAAS composite (Taylor and McLennan, 1985) reinforces the similarity of the Pavón samples to the average upper crust. The La_n/Yb_n ratios range from 4.08 to 7.86 (Table 5). In the discrimination diagram of Fig. 12b (McLennan et al., 1990), the Pavón Formation data plot

in a trend from the back-arc field to the superposed trailing edge and continental arc fields.

7.3. Nd isotopes

Isotopic methods can be very effective in obtaining information about the provenance of sediments or their metamorphic counterparts. The Nd isotope composition reflects the composition of the source rock and is not easily altered during weathering, transport, or diagenesis.

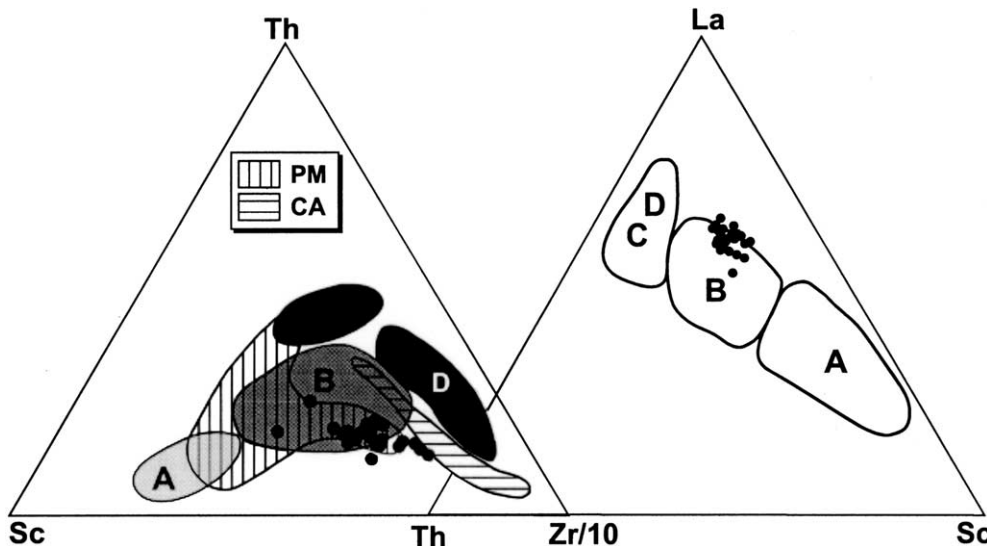


Fig. 11. Ternary diagrams La-Th-Sc and Sc-Th-Zr/10. Discrimination fields of tectonic setting are after Bhatia and Crook (1986). A = oceanic island arc; B = continental island arc; C = active continental margin; D = passive margin; PM = recent deep-sea turbidites derived from and deposited at a passive margin; CA = recent deep-sea turbidites derived from and deposited at a continental arc margin (data from McLennan et al., 1990). Most of the Pavón Formation data are consistent with a continental island arc derivation.

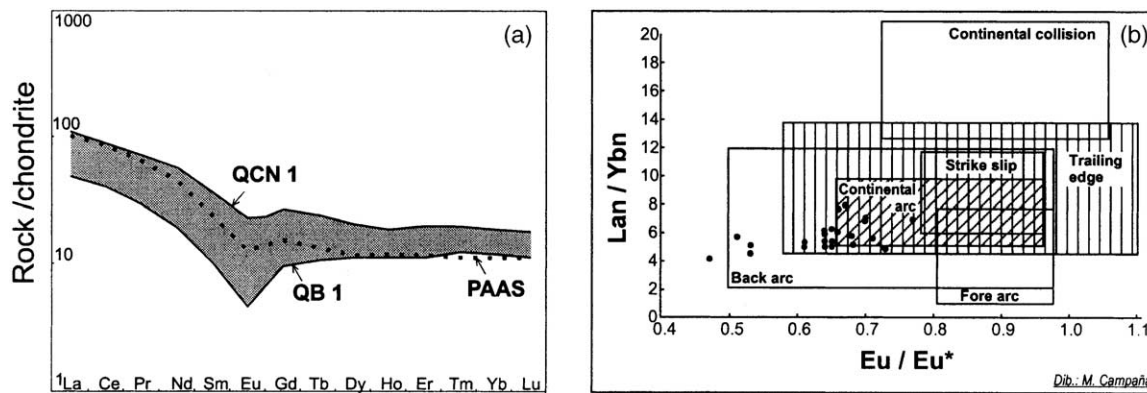


Fig. 12. (a) Chondrite-normalized REE spectra. The grey field indicates the REE patterns of the Pavón Formation samples, which are typical of upper crust compositions. PAAS = post-Archean average Australian shale composite. QCN1 and QB1 are samples in the upper and lower part of the REE spectra. (b) $\text{La}_{\text{n}}/\text{Yb}_{\text{n}}$ versus Eu/Eu^* diagram after McLennan et al. (1990).

Juvenile material can be recognized by higher εNd values than those of old upper crustal rocks. Sm–Nd isotope data also can be used to estimate the average crustal residence age (model age = T_{DM}) of the ultimate protolith or, if independent age data are available for the latter, its average εNd value.

T_{DM} crustal residence ages were calculated using the multistage model of DePaolo et al. (1991), which assumes a major fractionation of Sm/Nd when the crustal reservoir is first formed from the depleted mantle, followed by a single stage of crustal residence up to the time of magma generation/metamorphism. As shown in Table 6, the samples ($n = 5$) have a model age of 1.4–1.5 Ga, similar to the Grenvillian-age rocks of the Precordillera terrane (Kay et al., 1996; Pankhurst and Rapela, 1998), whereas the eastern, mature Gondwanan crust, where the Famatinian magmatic arc was emplaced, shows a concentration of older T_{DM} ages of 1.6–1.7 Ga (Pankhurst et al., 1998). The small number of analyzed samples may not be statistically meaningful but are consistent with derivation from the nearest Grenvillian-age crustal source: the Cerro La Ventana Formation, exposed in the Ponon Trehue area. Five granitoid samples (Cingolani, unpublished data) from this Formation have T_{DM} model ages (assuming crystallization at 1100 Ma) of 1.4–1.5 Ga, which are indistinguishable from those of the Pavón Formation (Table 6).

7.4. Summary of provenance indicators

The petrographical data presented herein plot in the recycled orogen and continental block fields of the QFL provenance diagram and indicate that the source area of the Pavón Formation had a typical upper crustal composition. The relatively high CIA (and CIW) documents significant major element changes due to pronounced and extended weathering of the source area,

so the major element compositions yield ambiguous results.

In the Pavón Formation sandstones, moderate Th/Sc and elevated Zr/Sc ratios reflect significant reworking and a clear input from upper crust igneous sources (silicic and intermediate magmatic precursors). Zircon is common heavy mineral, derived from granitic, volcanic, and metamorphic recycled sources. Major element distribution patterns suggest passive margin provenance, though disturbance due to weathering and recycling may have obscured the original signal. Immobile trace element diagrams are better source indicators for the Pavón Formation and suggest an active margin and island continental arc provenance. The REE distribution confirms a derivation from upper crustal source material composed chiefly of felsic components. Negative Eu anomalies also demonstrate intracrustal differentiation of the magmatic precursors by processes involving separation of plagioclase, such as partial melting or fractional crystallization, and εNd isotopic values further indicate the importance of the upper crust in their evolution. The Sm–Nd data give Nd T_{DM} model ages of 1.4–1.5 Ga for the provenance protolith, in agreement with the Grenville-age continental crust known in the Precordillera terrane.

8. Tectonic setting in the context of Precordillera terrane

In the Ponon Trehue region of the San Rafael block, it is possible to observe the Ordovician platform limestones, unconformably overlying the Grenville-age basement, such as the Cerro La Ventana Formation. The Cambrian–Lower Ordovician carbonate platform of the eastern and central Precordillera was drowned during the Middle Ordovician and covered by black shales (Keller, 1999). Arenigian–Lower Llanvirn K-bentonites record explosive volcanism, possibly of the Famatinian

Table 5
Selected geochemical ratios for Pavón Formation samples

| | QB1 | QB2 | QB3 | QB4 | QB5 | QB5r | QB6 | QM1 | QM2 | QM3 | QR1 | QR2 |
|---------|--------|--------|--------|--------|--------|--------|--------|--------|--------|--------|--------|--------|
| | QR3 | QR4 | QCN1 | PV1 | PV5 | PV8 | PV9 | PV10 | PV11 | PV13 | PV11' | PV12 |
| K/Rb | 0.02 | 0.03 | 0.03 | 0.03 | 0.03 | 0.03 | 0.03 | 0.03 | 0.03 | 0.03 | 0.02 | 0.02 |
| Rb/Sr | 0.79 | 0.74 | 0.77 | 1.18 | 2.9 | 2.83 | 1.14 | 2.91 | 1.48 | 1.01 | 1.99 | 2.3 |
| Ba/Rb | 21.88 | 37.67 | 13.29 | 9.08 | 5.51 | 5.85 | 4.73 | 4.37 | 4.56 | 5.96 | 3.44 | 2.98 |
| Ba/Sr | 17.3 | 27.93 | 10.19 | 10.73 | 15.97 | 16.55 | 5.41 | 12.74 | 6.75 | 6.04 | 6.85 | 6.86 |
| Th/U | 1.58 | 1.02 | 4.12 | 2.34 | 2.54 | 2.62 | 4.27 | 2.62 | 3.1 | 2.94 | 4.19 | 5.23 |
| Th/Sc | 0.79 | 0.64 | 0.74 | 0.64 | 0.52 | 0.59 | 0.58 | 0.54 | 0.63 | 0.63 | 0.83 | 0.74 |
| Zr/Sc | 40.13 | 36 | 28.8 | 23.85 | 17.16 | 18.06 | 22.57 | 19.06 | 18.79 | 23.79 | 11.68 | 12.25 |
| Zr/Hf | 41.15 | 40.5 | 35.56 | 36.05 | 37.91 | 35.7 | 36.74 | 35.47 | 35.54 | 36.59 | 32.65 | 33.11 |
| Zr/Nb | 47.91 | 37.67 | 24.83 | 22.79 | 18.95 | 18.72 | 26.33 | 20.89 | 20.39 | 21.62 | 9.61 | 10.17 |
| Zr/Y | 12.44 | 10.87 | 9.86 | 8.54 | 9.18 | 9.14 | 9.97 | 8.76 | 8.07 | 10.41 | 5.68 | 7.04 |
| Ti/Zr | 10.03 | 11.77 | 16.94 | 17.52 | 20.01 | 21.4 | 17.07 | 18.79 | 19.81 | 17.35 | 31.51 | 29.68 |
| Ti/Nb | 480.5 | 443.35 | 420.68 | 399.37 | 379.22 | 400.64 | 449.63 | 392.55 | 403.85 | 375.27 | 302.86 | 301.74 |
| Cr/Zr | 0.2 | 0.21 | 0.39 | 0.36 | 0.41 | 0.4 | 0.35 | 0.46 | 0.53 | 0.41 | 0.54 | 0.47 |
| Cr/V | 0.98 | 1.01 | 1.5 | 1.1 | 0.99 | 0.98 | 1.02 | 1.4 | 1.53 | 1.44 | 0.83 | 0.84 |
| Cr/Ni | | | 2.13 | 1.63 | 4.06 | 3.15 | 1.91 | 3 | 2.36 | 1.4 | 3.84 | 2.04 |
| Sc/Cr | 0.12 | 0.13 | 0.09 | 0.12 | 0.14 | 0.14 | 0.13 | 0.11 | 0.1 | 0.1 | 0.16 | 0.18 |
| V/Ni | | | 1.42 | 1.49 | 4.12 | 3.21 | 1.88 | 2.15 | 1.54 | 0.97 | 4.65 | 2.43 |
| Ni/Co | | | 1.27 | 1.48 | 1.83 | 2.17 | 1.57 | 1.27 | 1.74 | 1.78 | 1.15 | 2.07 |
| La/Th | 2.83 | 3.81 | 3.54 | 3.65 | 3.86 | 3.82 | 3.44 | 3.4 | 3.63 | 3.67 | 3.45 | 3.38 |
| La/Sc | 2.25 | 2.44 | 2.61 | 2.32 | 2.01 | 2.25 | 1.99 | 1.83 | 2.27 | 2.29 | 2.85 | 2.49 |
| La/Y | 0.7 | 0.74 | 0.89 | 0.83 | 1.07 | 1.14 | 0.88 | 0.84 | 0.98 | 1 | 1.39 | 1.43 |
| La/Yb | 6.04 | 6.61 | 7.31 | 7.33 | 8.88 | 8.9 | 7.46 | 7.88 | 8.66 | 8.47 | 11.63 | 11.19 |
| Lan/Ybn | 4.08 | 4.46 | 4.94 | 4.95 | 6 | 6.02 | 5.04 | 5.32 | 5.85 | 5.72 | 7.86 | 7.57 |
| Lan/Smn | 4.84 | 2.87 | 2.94 | 3.1 | 3.18 | 3.29 | 3.01 | 3.06 | 2.93 | 3.14 | 3.59 | 3.76 |
| Gdn/Ybn | 0.79 | 1.12 | 1.15 | 1.13 | 1.25 | 1.22 | 1.2 | 1.21 | 1.37 | 1.2 | 1.31 | 1.31 |
| Eu/Eu* | 0.47 | 0.53 | 0.64 | 0.65 | 0.66 | 0.64 | 0.68 | 0.64 | 0.64 | 0.68 | 0.67 | 0.66 |
| Sm/Nd | 0.17 | 0.22 | 0.22 | 0.22 | 0.21 | 0.21 | 0.22 | 0.22 | 0.22 | 0.21 | 0.2 | 0.2 |
| SREE | 93.17 | 124.1 | 144.1 | 165.3 | 203.5 | 199.3 | 154.3 | 157.7 | 172 | 173.3 | 271.5 | 244.9 |
| | | | | | | | | | | | | |
| | QR3 | QR4 | QCN1 | PV1 | PV5 | PV8 | PV9 | PV10 | PV11 | PV13 | PV11' | PV12 |
| K/Rb | 0.03 | 0.03 | 0.03 | 0.02 | 0.02 | 0.03 | 0.03 | 0.02 | 0.02 | 0.02 | 0.02 | 0.02 |
| Rb/Sr | 0.85 | 0.64 | 0.52 | 2.04 | 0.33 | 1 | 0.95 | 1.11 | 1.94 | 0.37 | 1.49 | 0.68 |
| Ba/Rb | 6.16 | 5.71 | 5.2 | 30.63 | 30.73 | 8.73 | 4.2 | 4.31 | 5.08 | 8.91 | 4.44 | 4.71 |
| Ba/Sr | 5.24 | 3.66 | 2.73 | 62.55 | 10.12 | 8.73 | 3.97 | 4.8 | 9.84 | 3.29 | 6.61 | 3.18 |
| Th/U | 3.25 | 4.32 | 3.53 | 3.11 | 1.6 | 2.1 | 3.93 | 3.94 | 2.83 | 3.2 | 4.51 | 2.58 |
| Th/Sc | 0.55 | 0.57 | 0.43 | 0.89 | 0.83 | 0.76 | 0.67 | 0.69 | 0.65 | 0.87 | 0.8 | 0.78 |
| Zr/Sc | 16.83 | 16.33 | 21.0 | 25.92 | 30.11 | 23.90 | 20.86 | 20.0 | 21.29 | 35.88 | 23.73 | 21.93 |
| Zr/Hf | 35.23 | 36.03 | 38.37 | 32.4 | 36.13 | 34.64 | 33.95 | 32.97 | 33.48 | 34.58 | 32.96 | 36.99 |
| Zr/Nb | 15.38 | 15.31 | 17.27 | 13.95 | 24.41 | 19.75 | 13.27 | 11.81 | 14.12 | 21.26 | 14.96 | 15.27 |
| Zr/Y | 9.1 | 8.54 | 10.93 | 8.66 | 10.84 | 8.82 | 10.07 | 8.4 | 8.37 | 10.83 | 9.3 | 6.33 |
| Ti/Zr | 20.08 | 22.37 | 23.9 | 21.45 | 15.2 | 20.49 | 24.23 | 25.62 | 22.61 | 14.96 | 19.55 | 18.94 |
| Ti/Nb | 308.88 | 342.46 | 412.9 | 299.21 | 371.04 | 404.79 | 321.55 | 302.58 | 319.35 | 317.96 | 292.45 | 289.31 |
| Cr/Zr | 0.93 | 0.52 | 0.73 | 0.37 | 0.31 | 0.46 | 0.54 | 0.55 | 0.6 | 0.39 | 0.47 | 0.54 |
| Cr/V | 2.55 | 1.32 | 2.01 | 0.99 | 1.14 | 1.62 | 1.53 | 1.5 | 1.09 | 1.42 | 1.58 | 0.61 |
| Cr/Ni | 0.61 | 2.65 | 4.56 | | 3.82 | 2.89 | 4.97 | 5.03 | 2.01 | 2.6 | 3.09 | 2.36 |
| Sc/Cr | 0.06 | 0.12 | 0.07 | 0.1 | 0.11 | 0.09 | 0.09 | 0.09 | 0.08 | 0.07 | 0.09 | 0.08 |
| V/Ni | 0.24 | 2 | 2.27 | | 3.36 | 1.79 | 3.25 | 3.36 | 1.84 | 1.84 | 1.96 | 3.89 |
| Ni/Co | 17.3 | 1.45 | 1.42 | | 0.85 | 1.09 | 1.52 | 1.38 | 2.47 | 1.72 | 2 | 4.12 |
| La/Th | 4.02 | 3.93 | 4.59 | 3.21 | 3.02 | 3.13 | 2.64 | 3.38 | 3.21 | 3.1 | 3.05 | 3.72 |
| La/Sc | 2.22 | 2.23 | 1.98 | 2.86 | 2.5 | 2.36 | 1.76 | 2.35 | 2.1 | 2.69 | 2.44 | 2.9 |
| La/Y | 1.2 | 1.17 | 1.03 | 0.96 | 0.9 | 0.87 | 0.85 | 0.99 | 0.83 | 0.81 | 0.96 | 0.84 |
| La/Yb | 9.95 | 10.31 | 10.22 | 8.35 | 7.43 | 7.76 | 7.11 | 8.19 | 7.42 | 7.29 | 7.79 | 9.14 |
| Lan/Ybn | 6.72 | 6.967 | 6.9 | 5.64 | 5.02 | 5.25 | 4.81 | 5.53 | 5.02 | 4.92 | 5.26 | 6.18 |
| Lan/Smn | 3.28 | 3.38 | 2.81 | 3.28 | 4.47 | 3.05 | 2.61 | 3 | 2.83 | 2.66 | 3.05 | 3.1 |
| Gdn/Ybn | 1.37 | 1.43 | 1.62 | 1.3 | 1.11 | 1.34 | 1.4 | 1.37 | 1.36 | 1.37 | 1.27 | 1.49 |
| Eu/Eu* | 0.7 | 0.7 | 0.77 | 0.51 | 0.53 | 0.61 | 0.73 | 0.71 | 0.66 | 0.61 | 0.65 | 0.65 |
| Sm/Nd | 0.21 | 0.2 | 0.22 | 0.2 | 0.19 | 0.2 | 0.22 | 0.21 | 0.22 | 0.22 | 0.21 | 0.2 |
| SREE | 207.2 | 171.8 | 201.1 | 188 | 112.2 | 132 | 153.4 | 196.6 | 167.1 | 123.7 | 202 | 214.7 |

Table 6

Sm-Nd isotope data for Pavón Formation samples

| | Sm | Nd | $^{147}\text{Sm}/^{144}\text{Nd}$ | $^{143}\text{Nd}/^{144}\text{Nd}$ | T_{DM} (Ga) | $\varepsilon\text{Nd}(0)$ | $\varepsilon\text{Nd}(\text{T})$ |
|--------------------------|-------|-------|-----------------------------------|-----------------------------------|----------------------|---------------------------|----------------------------------|
| Pavón Formation (455 Ma) | | | | | | | |
| PV 5 | 2.759 | 14.90 | .1120 | .512225 | 1.44 | -8.1 | -3.1 |
| QCB 1 | 1.899 | 12.17 | .0943 | .512177 | 1.43 | -9.0 | -3.1 |
| QCB 5 | 6.295 | 30.89 | .1232 | .512212 | 1.51 | -8.3 | -4.1 |
| QMoto2 | 5.520 | 26.08 | .1280 | .512248 | 1.40 | -7.6 | -3.7 |
| QCNEA1 | 7.260 | 33.90 | .1295 | .512418 | 1.10 | -4.3 | -.4 |

Notes: Analytical data by the Geochronological Center, University of Rio Grande do Sul, Porto Alegre, Brazil.

continental magmatic arc developed to the east in Gondwana (Huff et al., 1998). At c. 460 Ma, the Precordillera terrane accreted with Gondwana and produced syn-collisional deformation with western vergence and subsequent metamorphism on the eastern side of the Precordillera terrane (Astini et al., 1995; Astini, 1996; Ramos et al., 1998). Flexural extension and deformation by ductile thrusting at depth was followed by general uplift of areas in the western Sierras Pampeanas close to the suture (Ramos, 1999). At c.455 Ma (biostratigraphic age), the platform suffered extensional collapse, and Caradoc clastic sedimentary basins were initiated (Fig. 13).

In the San Rafael region, the Pavón Formation basin received clastic input mainly from the Grenville-age crust, as suggested by the Nd T_{DM} results. A subordinate contribution from the mature Gondwanan–Famatinian can be deduced from trace element information and a proportion of volcanic-type zircon crystals with a magmatic arc signature. Further isotopic and geochronological studies on detrital heavy minerals are needed to define the age and isotopic signature of the source and to test the different paleotectonic models proposed for the evolution of the western boundary of Gondwana.

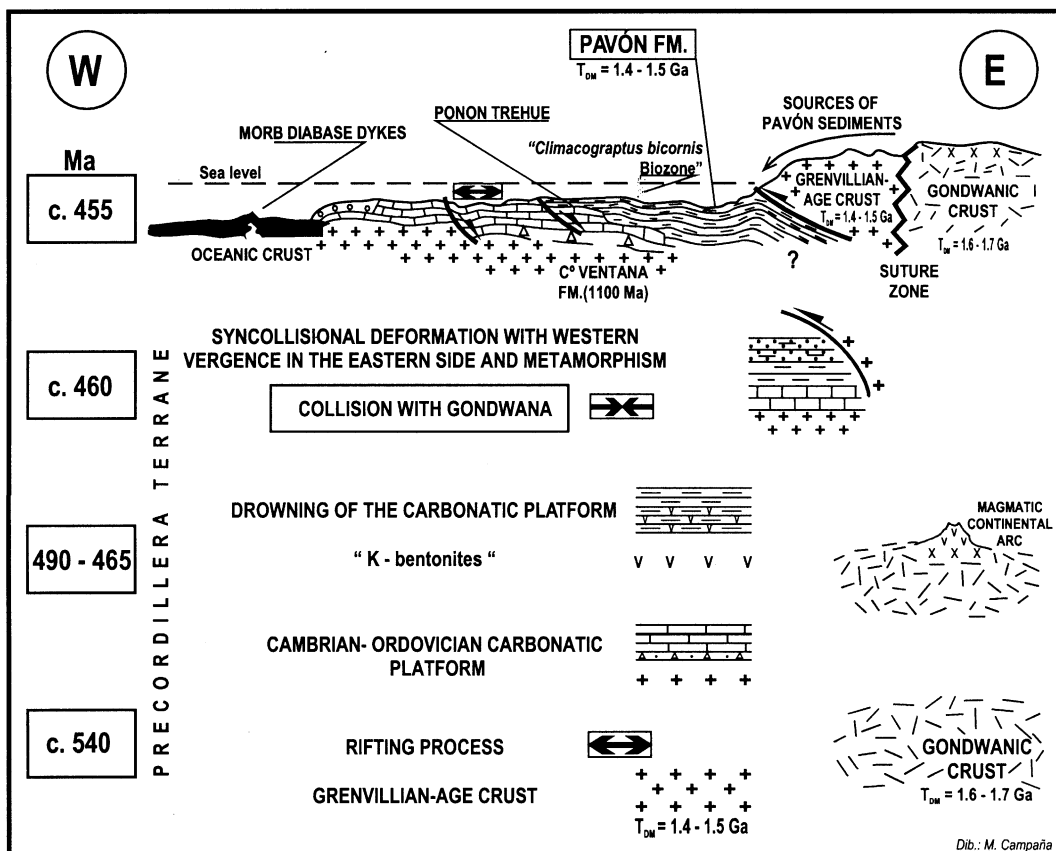


Fig. 13. Interpreted model following Astini et al. (1995) and Ramos (1999) for the tectonic and paleogeographic evolution of the Precordillera terrane from Precambrian to Ordovician times. The upper geological cross-section is displayed as the final interpretation of Pavón Formation depositional setting in the context of the San Rafael block.

9. Conclusions

The composition and provenance of the Pavón Formation has been assessed using integrated petrographical and geochemical studies. These rocks are dominantly quartz-feldspathic wackes, and QFL provenance data indicate a source with an average upper crustal composition. Two crust-type signatures (Grenvillian and Gondwanan) imply a complex provenance for the Pavón Formation sediments.

Detrital zircon grains are of mixed origin but include a component derived from a volcanic arc source, consistent with the results of trace element and REE indications of an active continental margin or continental island arc source. Nd T_{DM} model ages, in contrast, suggest bulk provenance from Grenvillian-age continental crust (such as the Cerro La Ventana Formation exposed nearby).

In the regional context of the evolution of the Precordillera terrane, our data support the conclusion that the Pavón Formation was deposited in a foreland basin generated after the accretion of the Precordillera with Gondwana and uplift by thrusting of the Grenville-age crust to the east.

Acknowledgements

Dr H. Lagiglia, Director of the Natural History Museum of San Rafael, Mendoza, provided important logistic help. We acknowledge useful discussions with H. Tickyj, A.M. Sato, and U. Zimmermann. Fieldwork was financed by a CONICET grant. L. Hernández kindly worked on some petrographical descriptions. Critical reviews by L. Spalletti, M. Keller, and R. Astini resulted in significant improvements to this paper. We are grateful to R. Pankhurst for very fruitful observations and suggestions on the final version. This a contribution to the IGCP project 436, ‘Pacific Gondwana margin.’

References

- Aceñolaza, F.G., Miller, H., Toselli, A.J., 2002. Proterozoic–Early Paleozoic evolution in western South America: a discussion. *Tectonophysics* 354, 121–137.
- Astini, R.A., 1996. Las Fases Diástróficas del Paleozoico Medio en la Precordillera del Oeste Argentino–Evidencias Estratigráficas. XII Congreso Geológico Argentino y III Congreso de Exploración de Hidrocarburos Actas 5, 509–526.
- Astini, R.A., 2002. Los conglomerados basales del Ordovícico de Ponón Trehue (Mendoza) y su significado en la historia sedimentaria del terreno exótico de Precordillera. *Revista Asociación Geológica Argentina* 57 (1), 19–34.
- Astini, R.A., Benedetto, J.L., Vaccari, N.E., 1995. The early Paleozoic evolution of the Argentine Precordillera as a Laurentian rifted, drifted, and collided terrane: a geodynamic model. *Geological Society America Bulletin* 107, 253–273.
- Bahlburg, H., 1998. The geochemistry and provenance of Ordovician turbidites in the Argentine Puna. *Geological Society, London, Special Publication* 142, 127–142.
- Bhatia, M.R., 1983. Plate tectonics and geochemical composition of sandstones. *Journal of Geology* 91 (6), 611–627.
- Bhatia, M.R., Crook, K.A.W., 1986. Trace element characteristics of graywackes and tectonic setting discrimination of sedimentary basins. *Contributions to Mineralogy and Petrology* 92, 181–193.
- Bock, B., McLennan, S.M., Hanson, G.N., 1994. Rare earth element redistribution and its effects on the neodymium isotope system in the Austin Glen member of the Normanskill Formation, New York, USA. *Geochimica et Cosmochimica Acta* 58, 5245–5253.
- Bock, B., Bahlburg, H., Wörner, G., Zimmermann, U., 2000. Tracing crustal evolution in the southern central Andes from Late Precambrian to Permian with geochemical and Nd and Pb isotope data. *Journal of Geology* 108, 515–535.
- Bordonaro, O., Keller, M., Lehnert, O., 1996. El Ordovícico de Ponón Trehue en la Provincia de Mendoza (Argentina): redefiniciones estratigráficas. *Actas XII Congreso Geológico Argentino y II Congreso de Exploración de Hidrocarburos* 1, 541–550.
- Cingolani, C.A., Varela, R., 1999. The San Rafael block, Mendoza (Argentina) Rb–Sr isotopic age of basement rocks. II South American Symposium on Isotope Geology, *Anales XXXIV SEGEMAR Actas* 23–26 Villa Carlos Paz, Córdoba.
- Cingolani, C.A., Cuerda, A., Manassero, M., 1999. Litoestratigrafía de los depósitos silicoclásticos ordovícicos del Cerro Bola, Bloque de San Rafael, Mendoza. XIV Congreso Geológico Argentino Actas 1, 409–413.
- Cingolani, C.A., Manassero, M., Abre, P., 2002. Geoquímica de elementos traza y tierras raras de las sedimentitas de la Formación Pavón, Ordovícico del Bloque de San Rafael, Mendoza. XV Congreso Geológico Argentino, CD-Rom version.
- Cuerda, A.J., Cingolani, C.A., 1998. El Ordovícico de la región del Cerro Bola en el Bloque de San Rafael, Mendoza: sus faunas graptolíticas. *Ameghiniana* 35 (4), 427–448.
- Cuerda, A.J., Cingolani, C.A., Manassero, M., 1998. Caradoc graptolite assemblages and facial relations from the Cerro Bola section, San Rafael block, Mendoza Province Argentina. Sixth International Graptolite Conference. IUGS Subcommission on Silurian Stratigraphy 23, 170–175. Madrid.
- Cullers, R.L., Chaudhuri, S., Kilbane, N., Koch, R., 1979. Rare earths in size fractions and sedimentary rocks of Pennsylvanian–Permian age from the mid-continent of the USA. *Geochimica et Cosmochimica Acta* 43, 1285–1302.
- Dalla Salda, L.H., Cingolani, C.A., Varela, R., 1992. Early Paleozoic belt of the Andes and southwestern South America: result of Laurentia–Gondwana collision? *Geology* 20, 517–520.
- DePaolo, D.J., Linn, A.M., Schubert, G., 1991. The continental crustal age distribution, Methods of determining mantle separation ages from Sm–Nd isotopic data and application to the southwestern United States. *Journal of Geophysical Research* 96 (B2), 2071–2088.
- Dessanti, R.N., 1945. Informe geológico preliminar sobre la Sierra Pintada, Departamento de San Rafael, Mendoza. Dirección Nacional de Geología y Minería, Carpeta 28, Buenos Aires (unpublished).
- Dessanti, R.N., 1956. Descripción geológica de la Hoja 27 c-Cerro Diamante (Provincia de Mendoza). Dirección Nacional de Geología y Minería Boletín 85, 1–79.
- Dickinson, W.R., Suczek, C., 1979. Plate tectonics and sandstone composition. *American Association of Petroleum Geologists Bulletin* 63, 2164–2192.
- Dickinson, W.R., Beard, S., Brakenbridge, F., Erjavec, J., Ferguson, R., Inman, K., Knepp, R., Lindberg, P., Ryberg, P., 1983. Provenance of North American Phanerozoic sandstones in relation to tectonic setting. *Geological Society of America Bulletin* 64, 233–235.
- Dott, R.H., 1964. Wacke, graywacke and matrix—what approach to immature sandstone classification. *Journal of Sedimentary Petrology* 34, 625–632.
- Einsele, G., 1991. Submarine mass flow deposits and turbidites. In: Einsele, (Ed.), *Cycles and Events in Stratigraphy*, Springer, Berlin, pp. 313–339.

- Floyd, P.A., Leveridge, B.E., 1987. Tectonic environment of the Devonian Gramscatho basin, south Cornwall: Framework mode and geochemical evidence from turbiditic sandstones. *Journal of the Geological Society, London* 144, 531–542.
- Floyd, P.A., Franke, W., Shail, R., Dörr, W., 1990. Provenance and depositional environment of Rhenohercynian synogenetic greywacke from the Giessen nappe, Germany. *Geologische Rundschau* 79, 611–626.
- González Díaz, E.F., 1981. Nuevos argumentos a favor del desdoblamiento de la denominada “Serie de la Horqueta” del Bloque de San Rafael. *Provincia de Mendoza. 8º Congreso Geológico Argentino Actas 3*, 241–256. San Luis.
- Harnois, L., 1988. The CIW index: A new chemical index of weathering. *Sedimentary Geology* 55, 319–322.
- Heredia, S., 1996. El Ordovícico del arroyo Ponón Trehue, sur de la provincia de Mendoza. *Actas 13º Congreso Geológico Argentino y 3º Congreso de Exploración de Hidrocarburos 1*, 601–605. Buenos Aires.
- Holmberg, E., 1948. Geología del Cerro Bola. Contribución al conocimiento de la tectónica de la Sierra Pintada. Secretaría de Industria y Comercio de la Nación. Dirección General de Industria y Minería. Boletín 69, pp. 313–361. Buenos Aires.
- Huff, W., Bergstrom, S.M., Kolata, D., Cingolani, C.A., Astini, R., 1998. Ordovician K-bentonites in the Argentine Precordillera: relations to Gondwana margin evolution. *Geological Society of London, Special Publication* 142, 107–126.
- Kay, S.M., Orrell, S., Abruzzi, J.M., 1996. Zircon and whole rock Nd–Pb isotopic evidence for a Grenville age and Laurentian origin for the basement of the Precordillera terrane in Argentina. *Geological Society of America South-Central section, abstracts with program* 28, 21–22.
- Keller, M., 1999. The Argentine Precordillera-sedimentary and plate tectonic history of a Laurentian crustal fragment in South America. *Geological Society of London, Special Publication* 341, 1–239.
- Loske, W., 1992. Sedimentologie, Herkunft und geotektonische Entwicklung paläozoischer Gesteine der Präkordillere West-Argentiniens. Münchner. *Geologische Hefte* 7, 155.
- Loske, W.P., 1994. The west-Argentine Precordillera: a Paleozoic back arc basin. *Zentralblatt Dt. Geologie Ges.* 145, 379–391.
- Manassero, M., Cingolani, C.A., Cuerda, A.J., Abre, P., 1999. Sedimentología, Paleoambiente y Procedencia de la Formación Pavón (Ordovícico) del Bloque de San Rafael, Mendoza. *Revista de la Asociación Argentina de Sedimentología* 6 (1–2), 75–90.
- Marquat, F.J., Menéndez, A.J., 1985. Graptofauna y edad de la Formación Lutitas del Cerro Bola, Sierra Pintada. Departamento San Rafael, Provincia de Mendoza, Argentina. Centro Cuyano de Documentación Científica, 11pp., Mendoza.
- Mass, R., McCulloch, M.T., 1991. The provenance of Archaean clastic metasediments in the Narreyer gneiss complex, Western Australia: trace element geochemistry, Nd isotopes, and U–Pb ages for detrital zircons. *Geochimica et Cosmochimica Acta* 55, 1915–1932.
- McLennan, S.M., 1989. Rare earth elements in sedimentary rocks: Influence of provenance and sedimentary process. *Mineralogical Society of America, Reviews in Mineralogy* 21, 169–200.
- McLennan, S.M., Taylor, S.R., McCulloch, M.T., Maynard, J.B., 1990. Geochemical and Nd–Sr isotopic composition of deep-sea turbidites: Crustal evolution and plate tectonic associations. *Geochimica et Cosmochimica Acta* 54, 2015–2050.
- McLennan, S.M., Hemming, S., McDaniel, D.K., Hanson, G.N., 1993. Geochemical approaches to sedimentation, provenance and tectonics. In: Johnsson, M.J., Basu, A. (Eds.), *Processes Controlling the Composition of Clastic Sediments*. Geological Society of America, Special Papers 285, pp. 21–40.
- Merodio, J.C., Spalletti, L.A., 1990. Geoquímica de pelitas: su empleo en la definición de ambientes sedimentarios y tectónicos para el Ordovícico de la Precordillera Occidental. *Revista Asociación Geológica Argentina* 45 (3–4), 336–345.
- Milodowski, A.E., Zalasiewicz, J.A., 1991. Redistribution of rare earth elements during diagenesis of turbidite/hemipelagite mudrock sequences of Llandovery age from central Wales. *Geological Society of America, Special Publication* 57, 101–124.
- Nesbitt, H.W., Young, G.M., 1982. Early Proterozoic climates and plate motions inferred from major element chemistry of lutites. *Nature* 199, 715–717.
- Nesbitt, H.W., Young, G.M., 1989. Formation and diagenesis of weathering profiles. *Journal of Geology* 97, 129–147.
- Núñez, E., 1979. Descripción geológica de la Hoja 28d. Estación Soitué, Provincia de Mendoza. Servicio Geológico Nacional. Boletín 166, 1–67. Buenos Aires.
- Pankhurst, R.J., Rapela, C.W., 1998. The proto-Andean margin of Gondwana: An introduction. *Geological Society of London, Special Publication* 142, 127–142.
- Pankhurst, R.J., Rapela, C.W., Saavedra, J., Baldo, E., Dahlquist, J., Pascua, I., Fanning, C.M., 1998. The Famatinian magmatic arc in the central Sierras Pampeanas: an Early to Mid-Ordovician continental arc on the Gondwana margin. *Geological Society of London, Special Publication* 142, 343–367.
- Poiré, D.G., Cingolani, C.A., Morel, E.M., 2002. Características sedimentológicas de la Formación Río Seco de los Castaños (Paleozoico) en el perfil de Agua del Blanco, Bloque de San Rafael, Mendoza. *15º Congreso Geológico Argentino, Calafate, CD-ROM version*.
- Ramos, V.A., 1999. Rasgos estructurales del territorio argentino. I. Evolución tectónica de la Argentina. *Geología Argentina. Anales* 29 (24), 715–784. Buenos Aires.
- Ramos, V.A., Mpodozis, C., Kay, S., Cortes, J.M., Palma, M.A., 1986. Paleozoic terranes of the Central Argentine-Chilean Andes. *Tectonics* 5, 855–880.
- Ramos, V.A., Dallmeyer, R., Vujovich, G., 1998. Time constraints on the Early Paleozoic docking of the Precordillera, central Argentina. *Geological Society of London, Special Publication* 142, 143–158.
- Roser, B.P., Korsch, R.J., 1986. Determination of tectonic setting sandstone-mudstone suites using SiO_2 content and $\text{K}_2\text{O}/\text{Na}_2\text{O}$ ratio. *Journal of Geology* 94 (5), 635–650.
- Roser, B.P., Korsch, R.J., 1988. Provenance signatures of sandstone-mudstone suites determined using discriminant function analysis of major-element data. *Chemical Geology* 67, 119–139.
- Sato, A.M., Tickyj, H., Llambías, E.J., Sato, K., 2000. The Las Matras tonalitic-trondjemitic pluton, central Argentina: Grenvillian-age constraints, geochemical characteristics, and regional implications. *Journal of South American Earth Sciences* 13, 587–610.
- Taylor, S.R., McLennan, S.M., 1985. *The Continental Crust: Its Composition and Evolution*. Blackwell, London, p. 312.
- Thomas, W.A., Tucker, R.D., Astini, R.A., 2000. Rifting of the Argentine Precordillera from southern Laurentia: Palinspastic restoration of basement provinces. *Geological Society of America, Abstracts with Programs*, 21–22.
- Valloni, R., Mezzardi, G., 1984. Compositional suites of terrigenous deep-sea sands of the present continental margins. *Sedimentology* 31, 353–364.
- Winchester, J.A., Floyd, P.A., 1977. Geochemical discrimination of different magma series and the differentiation products using immobile elements. *Chemical Geology* 20, 325–343.
- Zimmermann, U., 2000. The evolution of the Ordovician southern Puna basin in NW Argentina. A compilation. *IX Congreso Geológico Chileno 1*, 720–725. Puerto Varas, Chile.
- Zimmermann, U., Bahlburg, H., 1999. Provenance analysis of Ordovician clastic sedimentary rocks in the southern Puna (NW Argentina): New insights into the provenance evolution of western Gondwana. *XIV Congreso Geológico Argentino, Actas 1–78*, Salta.